Title

Severe Iron Metabolism Defects in Mice With Double Knockout of the Multicopper Ferroxidases Hephaestin and Ceruloplasmin.

Journal

Cellular and molecular gastroenterology and hepatology, 6(4)

ISSN

2352-345X

Authors

Fuqua, Brie K
Lu, Yan
Frazer, David M
et al.

Publication Date

2018

DOI

10.1016/j.jcmgh.2018.06.006

Peer reviewed

cmgh
CELLULAR AND MOLECULAR GASTROENTEROLOGY AND HEPATOLOGY

ORIGINAL RESEARCH

Severe Iron Metabolism Defects in Mice With Double Knockout of the Multicopper Ferroxidases Hephaestin and Ceruloplasmin

Brie K. Fuqua,[1,2,a] Yan Lu,[2,a] David M. Frazer,[2] Deepak Darshan,[2] Sarah J. Wilkins,[2] Linda Dunn,[2] Alex V. Loguinov,[1] Scott C. Kogan,[3] Pavle Matak,[4] Huijun Chen,[5] Joshua L. Dunaief,[6] Chris D. Vulpe,[1] and Gregory J. Anderson[2,7]

[1]Department of Nutritional Science and Toxicology, University of California, Berkeley, Berkeley, California; [2]Iron Metabolism Laboratory, QIMR Berghofer Medical Research Institute, Brisbane, Queensland, Australia; [3]Department of Laboratory Medicine and Helen Diller Comprehensive Cancer Center and Mouse Pathology Core, University of California, San Francisco, California; [4]Department of Pharmacology and Cancer Biology, Duke University, Duke University Medical Center, Durham, North Carolina; [5]Medical School, Nanjing University, Nanjing, Jiangsu Province, China; [6]FM Kirby Center for Molecular Ophthalmology, Scheie Eye Institute, University of Pennsylvania, Philadelphia, Pennsylvania; and [7]School of Chemistry and Molecular Bioscience, University of Queensland, Brisbane, Queensland, Australia

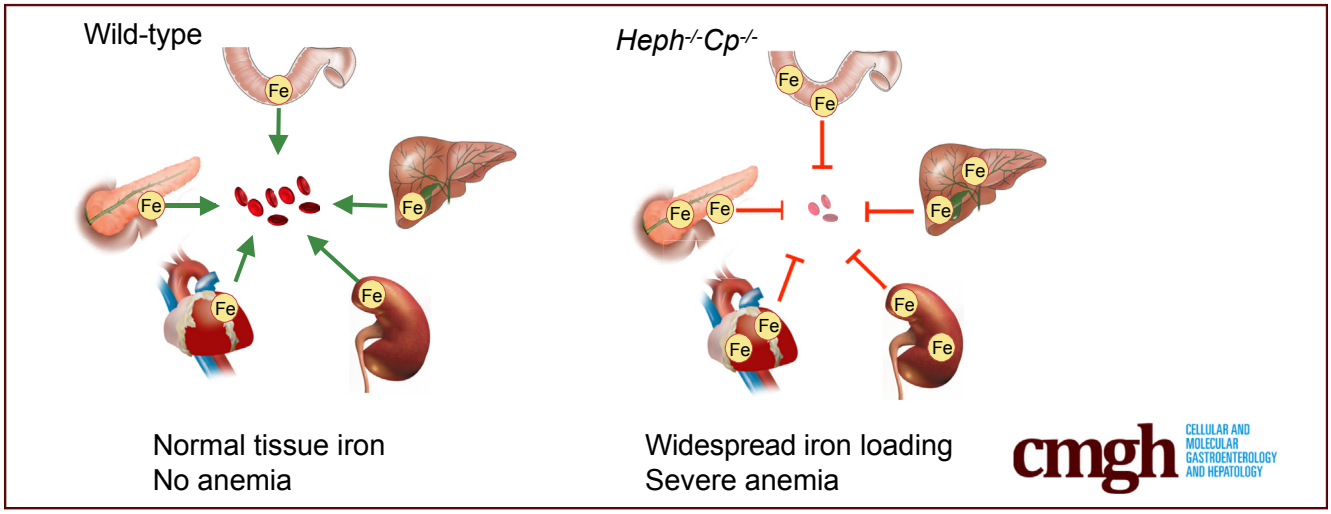

SUMMARY

Mice lacking 2 multicopper ferroxidases, hephaestin and ceruloplasmin, exhibit both tissue iron overload and severe iron deficiency anemia. These studies reveal the importance of these proteins and an extra-intestinal role of hephaestin in ensuring proper systemic iron distribution.

BACKGROUND & AIMS: Multicopper ferroxidases (MCFs) facilitate intestinal iron absorption and systemic iron recycling, likely by a mechanism involving the oxidization of Fe^{2+} from the iron exporter ferroportin 1 for delivery to the circulating Fe^{3+} carrier transferrin. Hephaestin (HEPH), the only MCF known to be expressed in enterocytes, aids in the basolateral transfer of dietary iron to the blood. Mice lacking HEPH in the whole body (*Heph*$^{-/-}$) or intestine alone (*Heph*$^{int/int}$) exhibit defects in dietary iron absorption but still survive and grow. Circulating ceruloplasmin (CP) is the only other known MCF likely to interact with enterocytes. Our aim was to assess the effects of combined deletion of HEPH and CP on intestinal iron absorption and homeostasis in mice.

METHODS: Mice lacking both HEPH and CP (*Heph*$^{-/-}$*Cp*$^{-/-}$) and mice with whole-body knockout of CP and intestine-specific deletion of HEPH (*Heph*$^{int/int}$*Cp*$^{-/-}$) were generated and phenotyped.

RESULTS: *Heph*$^{-/-}$*Cp*$^{-/-}$ mice were severely anemic and had low serum iron, but they exhibited marked iron loading in duodenal enterocytes, the liver, heart, pancreas, and other tissues. *Heph*$^{int/int}$*Cp*$^{-/-}$ mice were moderately anemic (similar to *Cp*$^{-/-}$ mice) but were iron loaded only in the duodenum and liver, as in *Heph*$^{int/int}$ and *Cp*$^{-/-}$ mice, respectively. Both double knockout models absorbed iron in radiolabeled intestinal iron absorption studies, but the iron was inappropriately distributed, with an abnormally high percentage retained in the liver.

CONCLUSIONS: These studies indicate that HEPH and CP, and likely MCFs in general, are not essential for intestinal iron absorption but are required for proper systemic iron distribution. They also point to important extra-intestinal roles for HEPH in maintaining whole-body iron homeostasis. *(Cell Mol Gastroenterol Hepatol 2018;6:405–427; https://doi.org/10.1016/j.jcmgh.2018.06.006)*

Keywords: Iron Deficiency Anemia; Iron Overload; Intestinal Iron Absorption; Non-Transferrin Bound Iron.

See editorial on page 470.

Multicopper ferroxidases (MCFs) enhance the efficiency of iron transport across biological membranes and are important for intestinal iron absorption and systemic iron recycling in vertebrates.[1] Evidence suggests that MCFs oxidize ferrous iron from the iron export protein ferroportin 1 (FPN1) (also known as SLC40A1), enabling the iron to bind to the ferric-specific iron carrier in the blood, transferrin (TF). The MCF ceruloplasmin (CP), which exists in both a soluble circulating form as well as in a GPI-linked form, assists in the release of iron from a variety of cell types including hepatocytes, macrophages, Sertoli cells, and astrocytes.[2–4] The membrane-bound MCF hephaestin (HEPH) exhibits highest expression in intestinal enterocytes and aids in the basolateral transfer of dietary iron to the circulation.[5] The primary role of zyklopen (also known as HEPHL1), the only other known mammalian MCF besides HEPH and CP, is currently unknown, although its tissue distribution suggests it could play a role in the brain, retina, kidney, and testes.[6]

To determine the importance of MCFs in intestinal iron absorption, we previously generated mice with whole-body (*Heph*$^{-/-}$) and intestine-specific (*Heph*$^{int/int}$) knockout of HEPH, the only MCF known to be expressed in intestinal enterocytes.[7] Ablation of HEPH perturbed, but did not abolish, intestinal iron absorption. Young knockout mice retained iron in their duodenal enterocytes and were anemic, but their anemia resolved with age as body iron requirements declined. The phenotype was much less severe than that reported for mice with whole-body knockout of FPN1 (unviable) or tamoxifen-induced postnatal ablation of FPN1 in the intestine, which results in a near complete block in intestinal iron absorption and the consequent development of very severe iron deficiency in young mice.[8] The survival and relatively mild phenotype of *Heph*$^{-/-}$ mice suggest that another MCF or some other ferroxidase may be able to partially compensate for loss of HEPH or, alternatively, that a ferroxidase is not absolutely required for intestinal iron absorption. In support of the former hypothesis, several studies in other cell types have indicated that FPN1 requires a ferroxidase to remain on the cell surface and properly export iron.[9–11] In addition, the ferric specificity of the iron carrier TF suggests a critical role for ferroxidases in the rapid and specific delivery of iron to this protein.[12]

The most likely ferroxidase that could at least partially compensate for HEPH ablation is the circulating form of the MCF CP. Although *Cp* is not known to be expressed at the mRNA level in intestinal enterocytes, CP has been detected by immunofluorescence in the lamina propria of duodenal villi and inside enterocytes.[13] Most notably, CP has been shown to augment intestinal iron absorption in mice in cases of extreme iron need.[13] CP also shares a high degree of sequence similarity with HEPH and co-immunoprecipitates with FPN1.[5,9] Conversely, zyklopen is not likely to play a role in intestinal iron absorption because no zyklopen expression has been detected in the small intestine or in the serum of mice.[6]

To test the potential contribution of CP to intestinal iron absorption in mice lacking HEPH, we generated mice with genetic ablation of both ferroxidases (*Heph*$^{-/-}$*Cp*$^{-/-}$). A mouse model lacking CP and expressing only the sex-linked anemia (*sla*) mutant form of HEPH (*Heph*$^{sla/sla}$*Cp*$^{-/-}$) was previously reported to be viable and to exhibit a tissue iron-loading phenotype.[14] However, no intestinal iron absorption studies were reported, and because the *sla* mutant may be a hypomorph and not equivalent to a null *Heph* allele, it was not possible to use that model to unequivocally determine whether HEPH and CP together are required for intestinal iron absorption or, if not, the importance of the role of CP. To differentiate between phenotypes caused by the ablation of HEPH in the intestine versus other tissues, we also generated a mouse model with whole-body knockout of CP but knockout of HEPH only in the intestine (*Heph*$^{int/int}$*Cp*$^{-/-}$).

Results

Heph$^{-/-}$*Cp*$^{-/-}$ Mice Are Visibly Small and Severely Anemic Throughout Life

Heph$^{-/-}$*Cp*$^{-/-}$ double knockout (DKO) mice and control littermates were generated by crossing wild-type (WT), *Heph*$^{-/-}$, *Heph*$^{-/-}$*Cp*$^{-/-}$, *Cp*$^{+/-}$, and *Cp*$^{-/-}$ male mice with *Heph*$^{+/-}$*Cp*$^{-/-}$ and *Heph*$^{+/-}$*Cp*$^{+/-}$ females. Because *Heph* is located on the X chromosome, the presence of the *Heph* knockout allele in male pups is only dependent on the dam. *Heph*$^{-/-}$*Cp*$^{-/-}$ pups were viable and could be easily differentiated from their littermates by eye both before weaning and throughout adulthood because of their small size and marked pallor (Figure 1*A* and *B*). The urine of the *Heph*$^{-/-}$*Cp*$^{-/-}$ mice, like that of WT mice made severely iron-deficient by an iron-deficient diet, was clear instead of yellow. In addition, whereas WT, *Heph*$^{-/-}$, and *Cp*$^{-/-}$ littermates developed yellow to brown iron deposits on their incisors, the teeth of *Heph*$^{-/-}$*Cp*$^{-/-}$ mice remained white throughout life (Figure 1*C*). Unlike the *Heph*$^{-/-}$*Cp*$^{-/-}$ mice, however, *Heph*$^{int/int}$*Cp*$^{-/-}$ mice, generated by crossing *Heph*$^{int/int}$*Cp*$^{-/-}$ males with *Heph*$^{fl/fl}$*Cp*$^{-/-}$ females, could not be reliably distinguished by eye from their

[a]Authors share co-first authorship.

Abbreviations used in this paper: **CP, ceruloplasmin; Cp$^{-/-}$, mice lacking CP in the whole body; DAB, 3,3′-diaminobenzidine; FDR, false discovery rate; FPN1, ferroportin 1; GI, gastrointestinal; HCl, hydrochloric acid; HEPH, hephaestin; Heph$^{-/-}$, mice lacking HEPH in the whole body; Heph$^{-/-}$Cp$^{-/-}$ or DKO, double-knockout mice lacking both HEPH and CP; Heph$^{fl/fl}$, mice with floxed Heph alleles; Heph$^{fl/fl}$Cp$^{-/-}$, mice with floxed Heph alleles and lacking CP in the whole body; Heph$^{int/int}$, mice lacking HEPH in the intestine alone; Heph$^{int/int}$Cp$^{-/-}$, mice lacking HEPH in the intestine alone and lacking CP in the whole body; Heph$^{sla/sla}$Cp$^{-/-}$, mice lacking CP in the whole body and expressing only the sla mutant form of HEPH; MCF, multicopper ferroxidase; NTBI, non-transferrin bound iron; PBS, phosphate-buffered saline; PCR, polymerase chain reaction; SD, standard deviation; sla, sex-linked anemia; TBST, Tris-buffered saline with 0.1% Tween-20; TF, transferrin; TIBC, total iron binding capacity; WT, wild-type.**

Most current article

2352-345X
https://doi.org/10.1016/j.jcmgh.2018.06.006

$Heph^{fl/fl}Cp^{-/-}$ littermates (although some were noted to have lighter teeth and paler paws than littermates), suggesting a milder phenotype (data not shown).

Weights of male $Heph^{-/-}Cp^{-/-}$ mice and non-DKO littermates were measured from 3–10 weeks of age, and $Heph^{-/-}Cp^{-/-}$ mice weighed less than their non-DKO littermates, with the difference becoming significant at 5 weeks of age (Figure 1*D*). $Heph^{-/-}Cp^{-/-}$ mice grew more slowly than their non-DKO littermates until approximately 8 weeks of age, when the rates became similar. On the basis of weights from a smaller sample of male animals at ages up to 30 weeks, $Heph^{-/-}Cp^{-/-}$ mice never catch up in weight to controls (data not shown). The weights of age-matched $Heph^{-/-}Cp^{-/-}$, $Heph^{int/int}Cp^{-/-}$, and littermate non-DKO males at 9–11 weeks of age, as well as 16- to 17-week-old WT mice fed an iron-deficient diet since weaning, were also compared (Figure 1*E*). No significant differences were detected in the weights of $Heph^{int/int}Cp^{-/-}$ mice and controls, but $Heph^{-/-}Cp^{-/-}$ mice weighed significantly less than non-DKO mice and were similar in weight to the WT males with severe diet-induced iron deficiency.

Hematology parameters were examined in male mice at 9–11 weeks of age (Figure 2*A*, Table 1) and at 20–23 weeks of age (Table 2). Male mice made severely iron-deficient by dietary means were also included for comparison. As reported previously, the anemia that affects juvenile $Heph^{-/-}$ mice was mostly resolved in adults at 9–11 weeks of age, although $Heph^{-/-}$ mice still had significantly smaller red cells with lower hemoglobin levels per cell than WT controls.[7] $Cp^{-/-}$ mice, as also reported previously, were mildly anemic at 9–11 weeks of age, with smaller red cells, less hemoglobin, and a lower hematocrit than WT mice.[15] At 20–23 weeks of age, results were generally similar to those at 9–11 weeks (Table 2). $Heph^{int/int}Cp^{-/-}$ mice were only examined at 9–11 weeks of age and were moderately anemic. They had significantly smaller red cells, lower hematocrit, less hemoglobin, and more platelets than WT controls but were not significantly different from $Cp^{-/-}$ mice except for having a higher platelet count.

In contrast, at both ages examined, $Heph^{-/-}Cp^{-/-}$ mice had a very severe hypochromic, microcytic anemia, similar to that of severely iron-deficient WT mice. They had approximately one-third the number of red cells of WT mice, and the cells were significantly smaller than all other genotypes, leading to a greatly reduced hematocrit. Total hemoglobin levels were less than one-fourth of that of controls. Because of the much smaller size of the red cells, the average concentration of hemoglobin in each cell was not significantly different than that of controls at 9–11 weeks of age. By 20–23 weeks of age, however, the average concentration of hemoglobin in each cell had dropped to levels significantly lower than controls. No reticulocytes were detected in any $Heph^{-/-}Cp^{-/-}$ mouse blood examined by the automatic analyzer, indicating that levels were below the limit of detection and that the mice possessed little capacity to generate new red cells. Platelet levels were, on average, more than 10 times that of WT. All $Heph^{-/-}Cp^{-/-}$ mice examined at 9–11 and 20–23 weeks of age had grossly enlarged spleens and hearts (data not shown), similar to observations in mice with diet-induced iron deficiency and consistent with severe anemia. There were no marked differences in the size of the hearts and spleens of $Heph^{int/int}Cp^{-/-}$ mice compared with controls.

$Heph^{-/-}Cp^{-/-}$ Mice Have Perturbed Tissue Iron Levels

$Heph^{-/-}Cp^{-/-}$ mouse serum iron levels were 11% of WT levels (Figure 2*B*, Table 3). $Heph^{-/-}Cp^{-/-}$ mice had elevated total iron binding capacities (TIBCs) (approximately twice that of WT) and TF saturation was 5% of WT. $Heph^{-/-}$ and $Cp^{-/-}$ single knockout mice also had lower serum iron levels (71% and 62% of WT levels, respectively) and lower TF saturations (58% and 59% WT levels, respectively) than WT.

Non-heme liver iron in 9- to 11-week-old males, as measured by colorimetric assay, was significantly greater in $Cp^{-/-}$ and $Heph^{-/-}Cp^{-/-}$ mice than WT controls (2–3 times that of WT), whereas levels in $Heph^{-/-}$ mice were just less than half that of WT (Figure 2*C*). Only 4 $Heph^{int/int}Cp^{-/-}$ mouse livers were available for non-heme liver iron analysis, and the values varied more than for any other genotype, but the average iron level was similar to that of $Cp^{-/-}$ and $Heph^{-/-}Cp^{-/-}$ mice. The expression of liver *Hamp1* mRNA was markedly reduced in both $Heph^{-/-}$ and $Heph^{-/-}Cp^{-/-}$ mice (4 orders of magnitude versus 3 orders of magnitude lower than WT, respectively). Notably, *Hamp1* mRNA levels in $Heph^{-/-}Cp^{-/-}$ mice were significantly greater than levels in $Heph^{-/-}$ mice. Levels in $Heph^{int/int}Cp^{-/-}$ and $Cp^{-/-}$ mice were similar to WT (Figure 2*D*).

Ferric iron in tissues from 9- to 11-week-old mice was visualized by using the semi-quantitative Perls' Prussian blue histochemical method. Strong iron loading was observed in the supranuclear region of duodenal enterocytes of $Heph^{-/-}$ mice, especially in cells at the villus tips, as has been reported previously (Figure 3). Little to no iron was observed in WT controls and $Cp^{-/-}$ enterocytes, but strong deposits were seen in all $Heph^{int/int}Cp^{-/-}$ and $Heph^{-/-}Cp^{-/-}$ samples, consistent with HEPH ablation in enterocytes in these mice. In the liver, the results were generally in agreement with the non-heme liver iron assay findings, with WT and $Heph^{-/-}$ mice showing the lowest levels of iron and $Cp^{-/-}$, $Heph^{int/int}Cp^{-/-}$, and $Heph^{-/-}Cp^{-/-}$ mice showing greater levels of iron, with the most variation in intensity between $Heph^{int/int}Cp^{-/-}$ livers. Staining was most intense in the periportal regions, with most of the iron loading in hepatocytes. The cells proximal to the central veins had little iron loading. There was no histologic evidence of extramedullary erythropoiesis in the liver. Punctate iron deposits were seen in the spleens of WT and $Cp^{-/-}$ mice and to a much lesser extent in $Heph^{-/-}$ mice. However, no iron was apparent in the spleens of any $Heph^{int/int}Cp^{-/-}$ mice or $Heph^{-/-}Cp^{-/-}$ mice. Consistent with their anemia, the enlarged spleens of the $Heph^{-/-}Cp^{-/-}$ mice were highly enriched in red pulp and exhibited marked immature erythroid hyperplasia. White pulp (lymphoid) was negligible.

The $Heph^{-/-}Cp^{-/-}$ mice, but no other mice, showed iron deposits in the heart, exocrine pancreas, adrenal glands, kidney, and Brunner's glands of the duodenum (Figures 3 and 4). In the heart, punctate iron deposits were present throughout the myocardial tissue, but no clear evidence of pathology was present at 9–11 weeks of age. In the

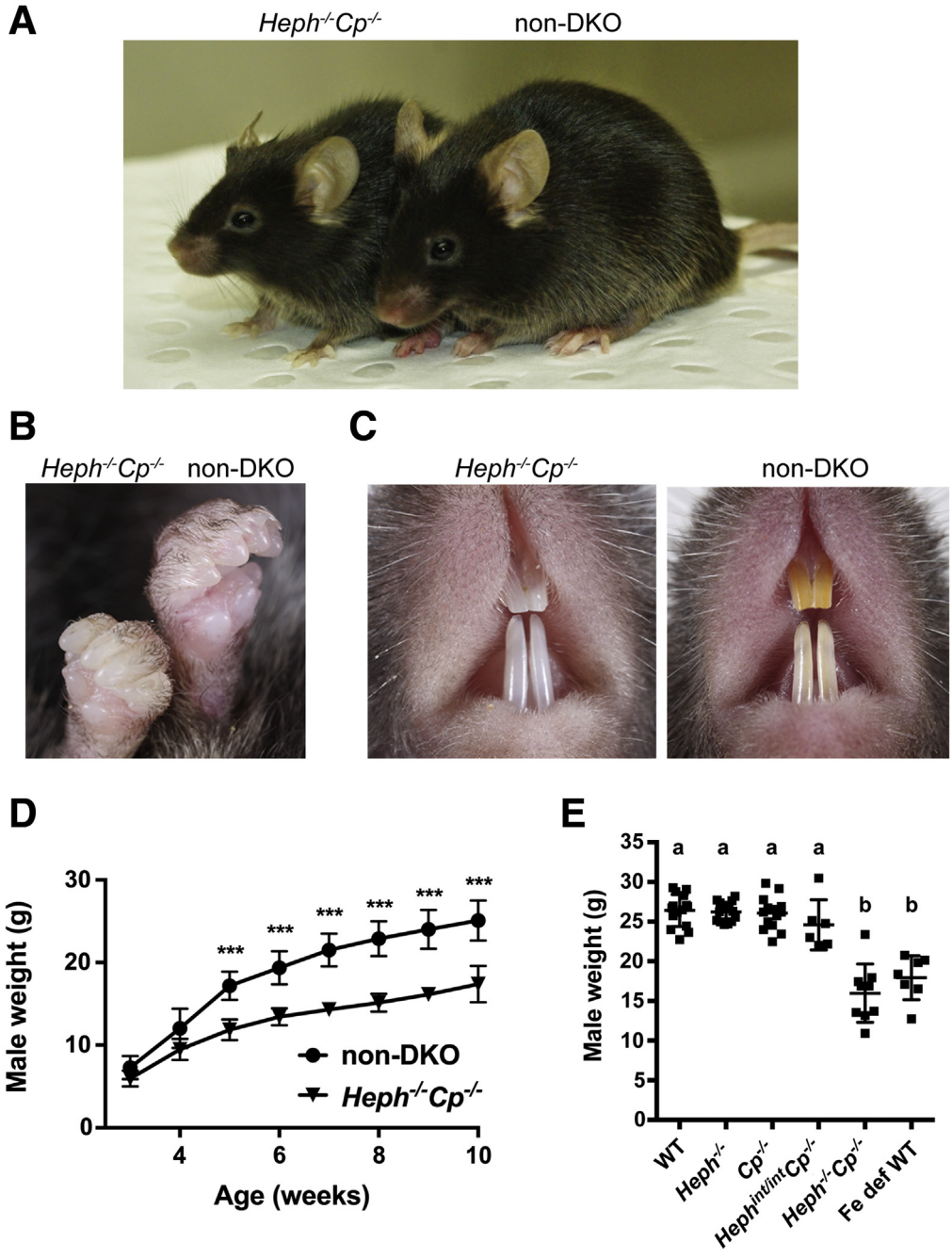

Figure 1. General phenotype of *Heph*$^{-/-}$*Cp*$^{-/-}$ mice. *Heph*$^{-/-}$*Cp*$^{-/-}$ mice are pale and small relative to all other genotypes examined. (*A*) General appearance of 2 adult littermate mice (*Heph*$^{-/-}$*Cp*$^{-/-}$ on *left* and non–double knockout (non-DKO) on *right*). (*B* and *C*) Paws of *Heph*$^{-/-}$*Cp*$^{-/-}$ mice are visibly small and pale, and their teeth lack visible iron deposits. (*D*) Growth rate of *Heph*$^{-/-}$*Cp*$^{-/-}$ and non-DKO littermate (*Heph*$^{-/-}$, WT, *Cp*$^{+/-}$, and *Cp*$^{-/-}$) male mice, N = 4–17 mice per age per group (***$P \leq .001$ by *t* test). (*E*) Weights of 9- to 11-week-old males fed standard chow and WT 16- to 17-week-old mice fed an iron-deficient diet since weaning (Fe def WT), N = 6–15 mice per genotype. For (*D*) and (*E*), data are presented as mean and SD. Groups with shared letters are not significantly different by Welch *t* test corrected for multiple comparisons with FDR (FDR-adjusted *P* value $>.05$).

pancreas, the Perls' reaction revealed strong punctate deposits of iron in the acinar exocrine cells but no visible deposits in the islets. Enhanced staining of a few samples with Perls' + 3,3′-diaminobenzidine (DAB), however, suggested that iron levels throughout the pancreas, including the islets, were greater in *Heph*$^{-/-}$*Cp*$^{-/-}$ mice than controls (data not shown). In *Heph*$^{-/-}$*Cp*$^{-/-}$ adrenal glands, iron loading was visible in a ring of cells near the outside edge of the tissue, and in females, on the outside edge but also in a ring of cells near the medulla/cortical junction (Figure 4). Iron loading was also uniquely present in the kidney of *Heph*$^{-/-}$*Cp*$^{-/-}$ mice in some cells of the medulla and cortex. Although there was no gross evidence of pathology in this tissue at this age, some *Heph*$^{-/-}$*Cp*$^{-/-}$ mice presented with one necrotic, fluid-filled kidney when euthanized. Abnormal iron loading was also visible by Perls' and Perls' + DAB staining in the choroid plexus region of the brains of *Heph*$^{-/-}$*Cp*$^{-/-}$ mice (data not shown). No marked iron staining was observed in 9- to 11-week-old mice from any groups in the skin, jejunum, ileum, lung, tongue, colon, cecum, stomach, skeletal muscle, gonad, brown fat, or white fat, and females showed similar overall staining patterns to males, with the exception of the medulla/cortical junction iron only seen in female adrenal glands. A small study of tissues (liver,

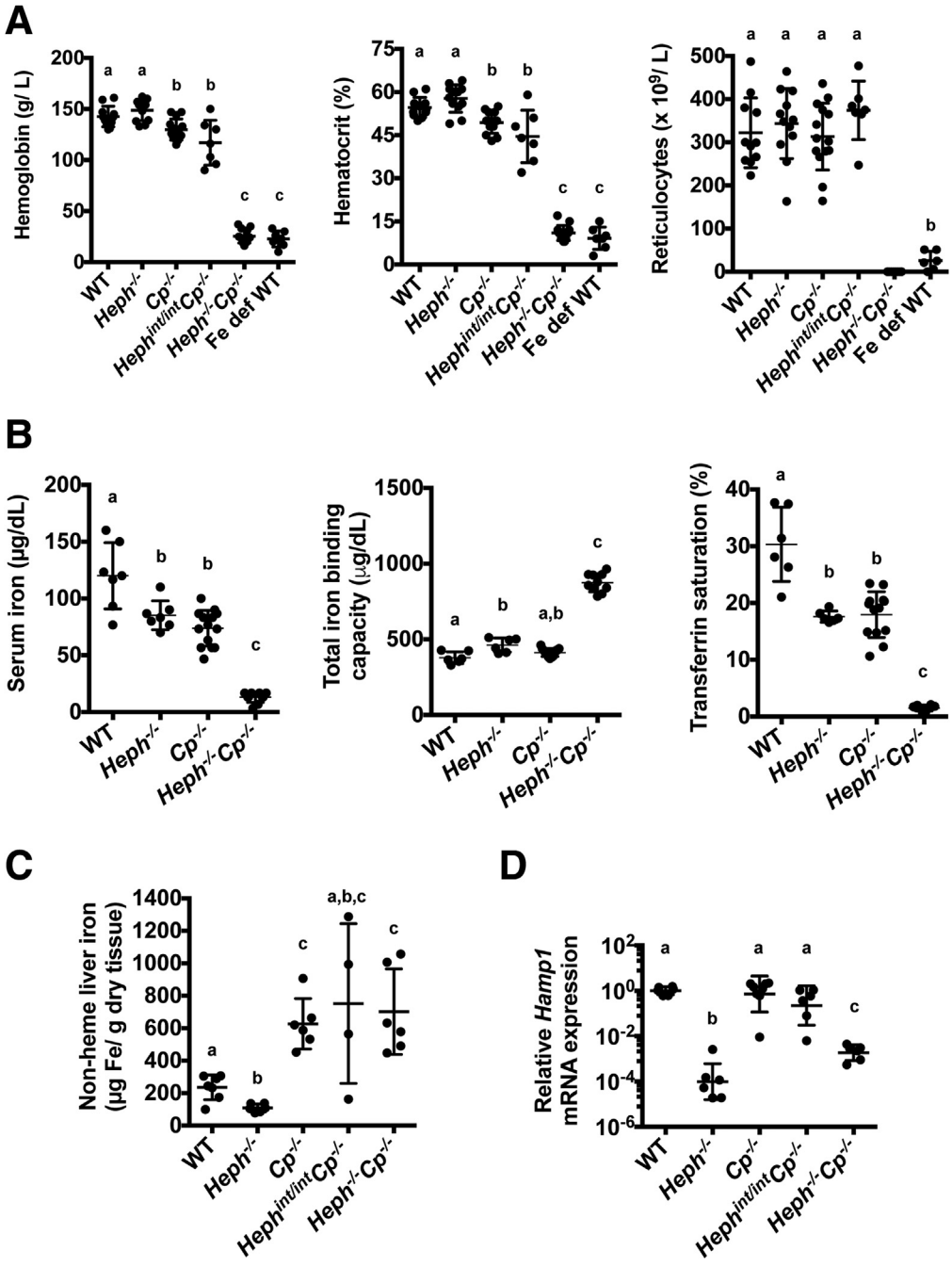

Figure 2. Hematology and iron status of *Heph*$^{-/-}$*Cp*$^{-/-}$ mice. Hematology, serum iron levels, and hepatic iron concentration were measured in 9- to 11-week-old male littermates on a chow diet. (*A*) Hemoglobin, hematocrit, and reticulocytes as measured by an automated analyzer, N = 7–14 mice per group. Hematology was also measured in six 16- to 17-week-old WT mice fed an iron-deficient diet since weaning (Fe def WT). (*B*) Serum iron, TIBC, and TF saturation as measured by a colorimetric ferrozine assay, N = 6–14 mice per genotype. (*C*) Hepatic non-heme liver iron as measured by a colorimetric assay, N = 4–7 mice per group. (*D*) Liver *Hamp1* mRNA expression normalized to expression of *Hprt* mRNA and then presented as a proportion of expression in WT mice. Individual normalized expression values (equal to $2^{-\Delta\Delta CT}$) for each mouse are shown on a log 10 scale, N = 6–8 mice per group. For each panel, data are presented as mean and SD, and groups with at least one shared letter are not significantly different as determined by Welch *t* test corrected for multiple comparisons with FDR (FDR-adjusted *P* value >.05).

pancreas, brown fat, duodenum, jejunum, ileum, lungs, spleen, and heart) from 20- to 26-week-old WT, *Heph*$^{-/-}$, *Cp*$^{-/-}$, and *Heph*$^{-/-}$*Cp*$^{-/-}$ males showed similar results to those of the 9- to 11-week-old mice, although the iron loading in the exocrine pancreas of the *Heph*$^{-/-}$*Cp*$^{-/-}$ mice was much more pronounced at this age.

Iron Absorption From the Intestine and Internal Distribution Is Altered in Heph$^{-/-}$*Cp*$^{-/-}$ *Mice*

Iron absorption and distribution in young adult and adult male mice.

The intestinal absorption of a radiolabeled dose of iron and the distribution of the dose retained were examined in 2 gavage studies with young adult (where iron requirements are higher) and adult (where iron requirements have stabilized) males. The first gavage study differed from the second in that the mean age of the mice was lower at the time of dosing (5.6 ± 0.5 weeks versus 13.1 ± 2.4 weeks). The results of both studies are presented in Table 4 and are shown graphically in Figure 5 (Study 1 in panels *A*–*C* and Study 2 in panels *D*–*F*). In these studies, mice were put on an iron-deficient diet for 1 week and then dosed by gavage with ^{59}Fe. Radioactive iron was measured by whole-body counting just after the gavage and then again 5 days later. In both studies, a greater percentage of the total ^{59}Fe dose was retained by *Heph*$^{-/-}$, *Cp*$^{-/-}$, and

Table 1. Hematology Parameters of 9- to 11-Week-Old Male Mice

Analysis	Genotype					
	WT	*Heph*$^{-/-}$	*Cp*$^{-/-}$	*Heph*$^{int/int}$ *Cp*$^{-/-}$	*Heph*$^{-/-}$*Cp*$^{-/-}$	Fe deficient WT
RBC ($\times 10^{12}$/L)	9.3 ± 0.7^{a}	10.7 ± 1.2^{b}	9.4 ± 1.0^{a}	9.5 ± 1.0^{a}	3.0 ± 0.7^{c}	2.1 ± 0.9^{c}
MCV (*fL*)	59 ± 2^{a}	54 ± 4^{b}	53 ± 4^{b,c}	47 ± 7^{c,d}	37 ± 2^{e}	43 ± 3^{d}
Hct (%)	55 ± 3^{a}	58 ± 5^{a}	49 ± 4^{b}	45 ± 9^{b}	11 ± 3^{c}	9 ± 4^{c}
Hb (*g/L*)	143 ± 10^{a}	149 ± 10^{a}	130 ± 10^{b}	117 ± 22^{b}	25 ± 7^{c}	23 ± 8^{c}
MCH (*pg*)	15.3 ± 0.4^{a}	14.0 ± 0.9^{b}	13.8 ± 0.7^{b,c}	12.3 ± 1.6^{c,d}	8.6 ± 2.0^{e}	11.2 ± 1.6^{d}
MCHC (*g/L*)	260 ± 11^{a}	258 ± 12^{a}	264 ± 12^{a}	265 ± 12^{a}	234 ± 67^{a}	263 ± 45^{a}
Reticulocytes ($\times 10^{9}$/L)	322 ± 81^{a}	343 ± 81^{a}	313 ± 77^{a}	374 ± 68^{a}	None detected	26 ± 22^{b}
Platelets ($x10^{9}$/L)	634 ± 109^{a}	835 ± 182^{b,c}	720 ± 297^{a,b}	1072 ± 325^{c}	6420 ± 1607^{d}	2392 ± 1525^{c}

NOTE. Hematology parameters of 9- to 11-week-old male littermates fed a chow diet and 16- to 17-week-old WT mice fed an iron-deficient diet since weaning (Fe deficient WT). Mean ± SD. Results for each analysis were examined by Welch *t* test and corrected for multiple comparisons with FDR. For each analysis, groups that share at least 1 superscript letter are not significantly different (FDR-adjusted *P* value >.05). For each analysis in rows 1–6 and 8, N = 11 WT, 12 *Heph*$^{-/-}$, 14 *Cp*$^{-/-}$, 7 *Heph*$^{int/int}$*Cp*$^{-/-}$, 13 *Heph*$^{-/-}$*Cp*$^{-/-}$, and 7 Fe deficient WT mice. For reticulocytes (row 7), N values were the same as for rows 1–6 and 8 with the exception of N = 12 *Heph*$^{-/-}$*Cp*$^{-/-}$ mice (reticulocytes results were not given on the report for 1 mouse) and N = 6 Fe deficient WT mice (1 extreme outlier was excluded).
Hb, hemoglobin; Hct, hematocrit; MCH, mean cell hemoglobin; MCHC, mean cell hemoglobin concentration; MCV, mean cell volume; RBC, red blood cells.

Heph$^{-/-}$*Cp*$^{-/-}$ mice than by WT mice. Retention in *Heph*$^{-/-}$ mice was not significantly different than in WT in Gavage Study 1, but the power to detect a difference was low because there were only 3 *Heph*$^{-/-}$ mice in that study. *Heph*$^{-/-}$*Cp*$^{-/-}$ mice tended to show greater iron retention than the other genotypes.

To determine how the iron dose was distributed, the mice were then euthanized, and the percentage of the retained dose in the gastrointestinal (GI) tract (esophagus just above the stomach to the anus, attached mesentery, and intestinal contents), liver, 200 μL whole blood, kidney, pancreas, spleen, and in the rest of the carcass (referred to as "remaining carcass" in this experiment) was examined. In Gavage Study 1, the pancreas was not excised from the GI tract, so individual results for those 2 tissues are not available. Clear differences in the distribution of the absorbed iron were found (Figure 5*B* and *E*, Table 4). Of the ^{59}Fe retained in the whole animal, more iron was in the GI tract in the *Heph*$^{-/-}$*Cp*$^{-/-}$ mice than any of the other groups, which all had GI retention similar to WT. The fraction of the retained dose in the GI tract (not including the pancreas in this case to ensure that only intestinal iron was assessed) that was in the duodenum was measured in Study 2 and was not significantly different from WT for any genotype, but the individual results were highly variable. Of note, after excluding the GI tract from whole-body iron retention, *Heph*$^{-/-}$*Cp*$^{-/-}$ mice still had retained more of the iron dose than WT mice (Table 4, "Whole body retention, minus GI (% of dose)").

Table 2. Hematology Parameters of 20- to 23-Week-Old Male Mice

Analysis	Genotype			
	WT	*Heph*$^{-/-}$	*Cp*$^{-/-}$	*Heph*$^{-/-}$*Cp*$^{-/-}$
RBC ($\times 10^{12}$/L)	10 ± 0.5^{a}	9.2 ± 0.5^{a}	9.7 ± 1.6^{a}	3.4 ± 0.8^{b}
MCV (*fL*)	57 ± 3^{a}	54 ± 1^{b}	47 ± 1^{c}	38 ± 1^{d}
Hct (%)	57 ± 5^{a}	50 ± 3^{b}	45 ± 8^{b}	13 ± 3^{c}
Hb (*g/L*)	150 ± 8^{a}	139 ± 6^{a,b}	125 ± 22^{b}	28 ± 11^{c}
MCH (*pg*)	15.0 ± 0.3^{a}	15.0 ± 0.4^{a}	12.8 ± 0.4^{b}	8.0 ± 1.4^{c}
MCHC (*g/L*)	264 ± 10^{a}	278 ± 8^{b}	275 ± 5^{b}	213 ± 42^{c}
Reticulocytes ($\times 10^{9}$/L)	312 ± 36^{a}	361 ± 79^{a}	349 ± 73^{a}	None detected
Platelets ($\times 10^{9}$/L)	657 ± 114^{a}	578 ± 104^{a}	676 ± 110^{a}	6694 ± 1501^{b}

NOTE. Hematology parameters of 20- to 23-week-old males fed a chow diet. Mean ± SD. Results for each analysis were examined by Welch *t* test and corrected for multiple comparisons with FDR. For each analysis, groups that share at least 1 superscript letter are not significantly different (FDR-adjusted *P* value >.05). N = 8 WT, 4 *Heph*$^{-/-}$, 7 *Cp*$^{-/-}$, and 6 *Heph*$^{-/-}$*Cp*$^{-/-}$ mice.
Hb, hemoglobin; Hct, hematocrit; MCH, mean cell hemoglobin; MCHC, mean cell hemoglobin concentration; MCV, mean cell volume; RBC, red blood cells.

Table 3. Serum Iron, TIBC, and TF Saturation

Analysis	Genotype				
	WT	*Heph*$^{-/-}$	*Cp*$^{-/-}$	*Heph*$^{-/-}$*Cp*$^{-/-}$	Fe deficient WT
Serum iron (*μg/dL*)	120 ± 29[a]	85 ± 13[b]	74 ± 16[b]	13 ± 5[c]	30
TIBC (*μg/dL*)	379 ± 39[a]	462 ± 47[b]	413 ± 27[a,b]	874 ± 60[c]	527
TF saturation* (%)	30.3 ± 6.5[a]	17.6 ± 1.0[b]	18.0 ± 4.0[b]	1.5 ± 0.5[c]	5.7

NOTE. Serum iron, TIBC, and TF saturation as measured by ferrozine colorimetric assay in 9- to 11-week-old male littermates fed a chow diet and WT mice fed an iron-deficient diet for 6 weeks since weaning (Fe deficient WT). Mean ± SD; if no SD, only 1 animal was tested. Results for each analysis were examined by Welch *t* test and corrected for multiple comparisons with FDR. For each analysis, groups that share at least 1 superscript letter are not significantly different (FDR-adjusted *P* value >.05). Fe deficient WT mice were not included in the statistical analyses. N = 7 WT, 7 *Heph*$^{-/-}$, 14 *Cp*$^{-/-}$, and 10 *Heph*$^{-/-}$*Cp*$^{-/-}$ mice. For TIBC and TF saturation, N = 6 WT, 6 *Heph*$^{-/-}$, 13 *Cp*$^{-/-}$, and 10 *Heph*$^{-/-}$*Cp*$^{-/-}$ mice.
*TF saturation assumes any iron detected in this assay is bound to TF in vivo.

In both studies, a significantly lower percentage of the retained dose was present in 200 μL of whole blood from *Heph*$^{int/int}$*Cp*$^{-/-}$ and *Heph*$^{-/-}$*Cp*$^{-/-}$ mice than WT, *Heph*$^{-/-}$, and *Cp*$^{-/-}$ mice. Furthermore, blood ^{59}Fe levels in *Heph*$^{-/-}$*Cp*$^{-/-}$ mice were much lower than in *Heph*$^{int/int}$*Cp*$^{-/-}$ mice. When red cells and serum were separated, no radiation could be detected in the serum fraction from any of the mice, indicating that essentially all of the radioactive iron in the blood was incorporated into red cells. We next estimated the percentage of the total retained dose that was present in the total blood volume (the total fraction incorporated into red blood cells) by assuming that approximately 6% of each mouse's total body weight was blood (Figure 5*C* and *F*, Table 4).[16] By this method, *Heph*$^{-/-}$*Cp*$^{-/-}$ mice only incorporated 10% ± 2% and 10% ± 3% of the retained dose into circulating red cells, whereas WT mice incorporated 72% ± 22% and 68% ± 17%, in Studies 1 and 2, respectively. *Heph*$^{-/-}$ and *Cp*$^{-/-}$ mice incorporated levels similar to WT, whereas *Heph*$^{int/int}$*Cp*$^{-/-}$ mice incorporated 50% ± 12% and 45% ± 10%, in Studies 1 and 2, respectively.

A significantly greater fraction of the retained ^{59}Fe was present in the livers of *Heph*$^{int/int}$*Cp*$^{-/-}$ and *Heph*$^{-/-}$*Cp*$^{-/-}$ mice than in the livers of WT, *Heph*$^{-/-}$, and *Cp*$^{-/-}$ mice. *Heph*$^{int/int}$*Cp*$^{-/-}$ and *Heph*$^{-/-}$*Cp*$^{-/-}$ mice had similar fractions of the retained dose in their livers. Tissue weights were measured in Study 2, and *Heph*$^{-/-}$*Cp*$^{-/-}$mice had on average a 1.2–1.4 times higher fraction of their body weight in their livers than the other genotypes (which had similar levels), but this weight difference could not account for the greater fraction of retained iron in their livers (Figure 6).

Overall, very little of the radiolabeled iron dose was detected in the kidneys, spleen, or pancreas of any mouse, and levels were close to the limit of detection. However, *Heph*$^{-/-}$*Cp*$^{-/-}$ mice had a significantly greater fraction of retained iron in their spleen and pancreas than the other genotypes. The spleens of *Heph*$^{-/-}$*Cp*$^{-/-}$ mice made up approximately 7 times more of their body weight than in the other groups, so this may explain the greater fraction of labeled iron in that tissue (Figure 6). Pancreas weights were not measured. None of the groups had significantly different fractions of the labeled iron in their kidneys, and the percentage of body weight in the kidneys was similar for all genotypes (Figure 6). The percentage of the retained iron dose in the remaining carcass was significantly lower in the *Heph*$^{int/int}$*Cp*$^{-/-}$ and *Heph*$^{-/-}$*Cp*$^{-/-}$ mice than WT.

Intestinal Iron Absorption and Distribution in Suckling Mice

Because *Heph*$^{-/-}$*Cp*$^{-/-}$ mice could be readily distinguished from their non-DKO littermates before weaning, either intestinal iron absorption was impaired and/or iron was inappropriately distributed during suckling. Iron absorption was measured in male and female juvenile littermates (15 days old) 4 days after gavage of a radiolabeled iron dose (Figure 7*A* and *B*). The *Heph*$^{-/-}$*Cp*$^{-/-}$ mice (N = 4) were identified by their pale color, and the non-DKO littermates (N = 8) contained a mix of *Heph* knockout, *Cp* knockout, and WT alleles. The mice were returned to their mother after dosing. There was large variation in the amount of iron retained in the *Heph*$^{-/-}$*Cp*$^{-/-}$ pups, and the amount retained (60% ± 28%) was not significantly different from littermate non-DKO controls (85% ± 11%; Figure 7*A*). However, there were significant differences in the distribution of the retained iron in *Heph*$^{-/-}$*Cp*$^{-/-}$ juveniles compared to controls (Figure 7*B*). Of the dose retained in *Heph*$^{-/-}$*Cp*$^{-/-}$ pups after 4 days, 23% ± 5% was in the GI tract, 38% ± 7% was in the liver, 2% ± 1% was in the spleen, and 37% ± 2% was in the rest of the carcass. Of the dose retained in the non-DKO littermates, 5% ± 3% was in the GI tract, 8% ± 6% was in the liver, 1% ± 1% was in the spleen, and 87% ± 6% was in the rest of the carcass. Like adult *Heph*$^{-/-}$*Cp*$^{-/-}$ mice, the *Heph*$^{-/-}$*Cp*$^{-/-}$ pups had grossly enlarged spleens. These results suggest impaired transfer of iron from the intestine of the *Heph*$^{-/-}$*Cp*$^{-/-}$ juveniles to the body, as well as abnormal retention of the transferred iron in the liver, as was observed in adults.

Iron Absorption From a Ligated Duodenal Gut Segment

The amount of iron taken up and transferred specifically by the duodenum, as well as the distribution of this iron after only a short period post-transfer, was determined by measuring radiolabeled iron absorption from ligated

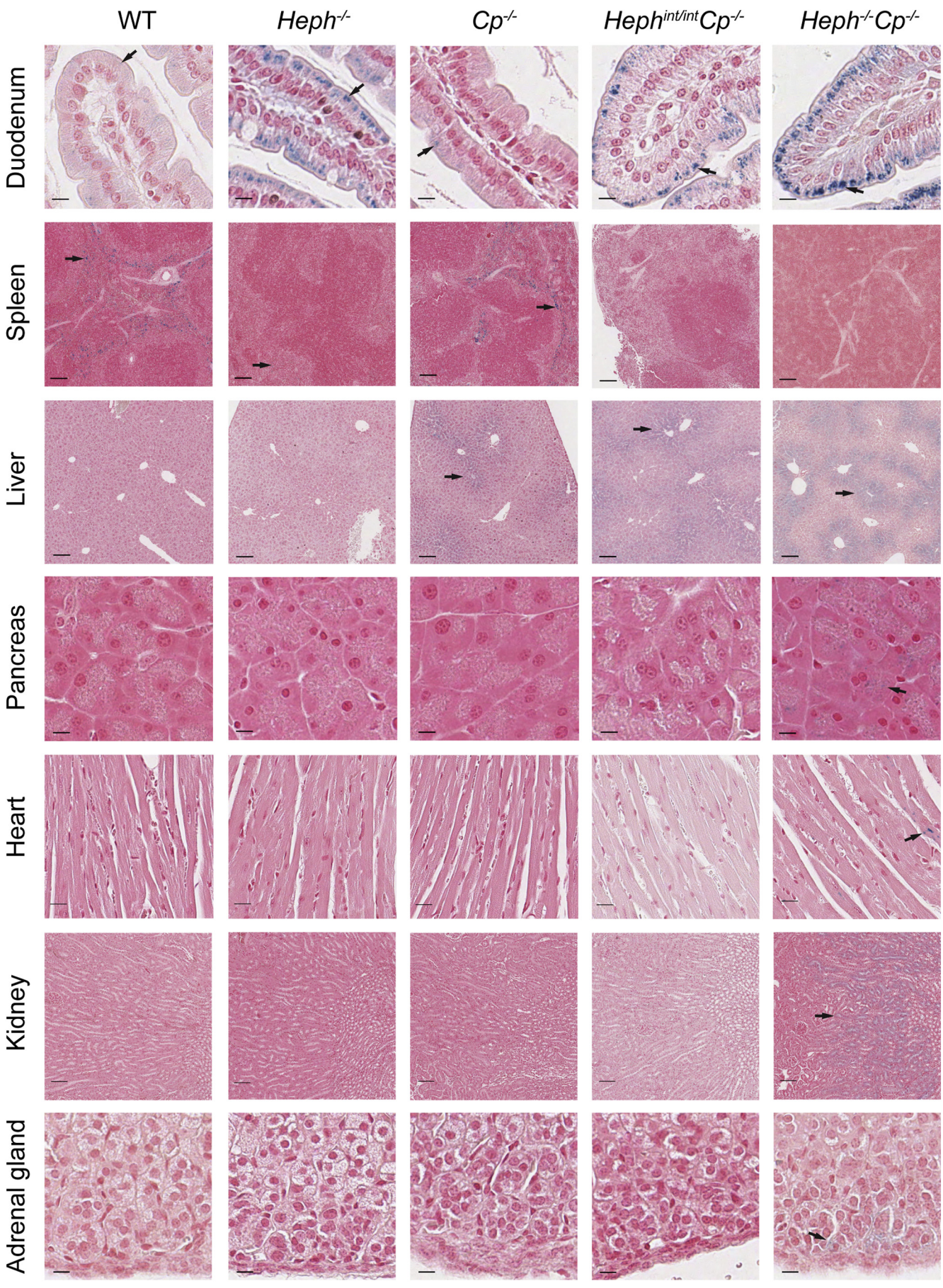
WT
Heph-/-
Cp-/-
Hephint/intCp-/-
Heph-/-Cp-/-
Duodenum
Spleen
Liver
Pancreas
Heart
Kidney
Adrenal gland

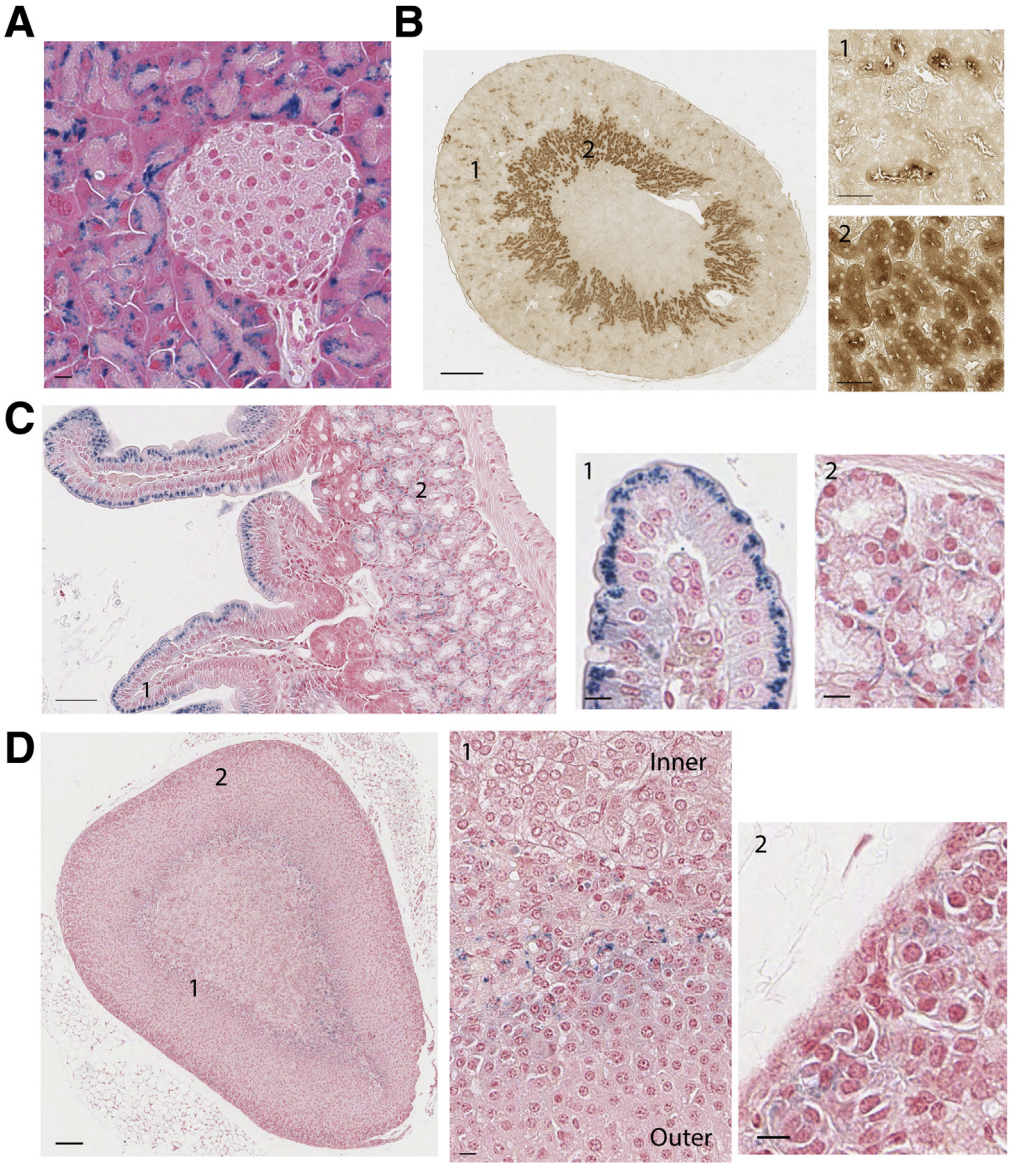

Figure 4. Region-specific iron loading in the pancreas, kidney, duodenum, and adrenal gland of *Heph*$^{-/-}$*Cp*$^{-/-}$ mice. (*A*) Perls' Prussian blue staining of the pancreas of a 26-week-old male *Heph*$^{-/-}$*Cp*$^{-/-}$ mouse showing punctate blue iron deposits in acinar cells and an absence of deposits in the islet cells (scale bar 10 μm, original magnification $\times$40). (*B*) Perls' + DAB enhanced staining of the kidney of a 10-week-old male *Heph*$^{-/-}$*Cp*$^{-/-}$ mouse showing iron loading (*brown*) in some cells in regions 1 and 2 (*left image*: scale bar 500 μm, original magnification $\times$2). Higher magnification images (scale bar 50 μm, original magnification $\times$20) show cells in the cortex (*1*, *top right*) and in the medulla (*2*, *bottom right*). (*C*) Perls' staining of the duodenum of a 10-week-old male *Heph*$^{-/-}$*Cp*$^{-/-}$ mouse showing iron loading of some cells in regions 1 and 2 (*left image*: scale bar 50 μm, original magnification $\times$10). Higher magnification images show punctate iron deposits in duodenal enterocytes near a villus tip (*middle image*: scale bar 10 μm, original magnification $\times$40) and in the Brunner's glands (*right image*: scale bar 10 μm, original magnification $\times$40). (*D*) Perls' staining of an adrenal gland in a 10-week-old female *Heph*$^{-/-}$*Cp*$^{-/-}$ mouse, with blue iron deposits in some cells in regions 1 and 2 (*left image*: scale bar 100 μm, original magnification $\times$4). Higher magnification images show iron deposits in cells near the junction of the cortex and medulla (*middle image*: scale bar 10 μm, original magnification $\times$40) and on the adrenal gland periphery (*right image*: scale bar 10 μm, original magnification $\times$40).

Figure 3. (***See previous page***). **Tissue histology and Perls' Prussian blue iron staining in knockout mice.** Representative photomicrographs are shown for duodenum, spleen, liver, pancreas, heart, kidney, and adrenal gland tissues of male 9- to 11-week-old WT, *Heph*$^{-/-}$, *Cp*$^{-/-}$, *Heph*$^{int/int}$*Cp*$^{-/-}$, and *Heph*$^{-/-}$*Cp*$^{-/-}$ mice. For each tissue where iron staining (*blue*) was typically observed for a given genotype, *1 arrow* points to an example in this region. Length of scale bars at bottom left of each image and original magnification of each image are as follows: duodenum (10 μm, $\times$40), spleen (100 μm, $\times$4), liver (100 μm, $\times$4), exocrine pancreas (10 μm, $\times$40), heart (20 μm, $\times$20), kidney (100 μm, $\times$4), and adrenal gland periphery (10 μm, $\times$40).

Table 4. Radiolabeled Iron Absorption and Distribution Analysis

		Genotype				
	Study	WT	*Heph*$^{-/-}$	*Cp*$^{-/-}$	*Heph*$^{int/int}$*Cp*$^{-/-}$	*Heph*$^{-/-}$*Cp*$^{-/-}$
Whole-body retention (% *of dose*)	1	27 ± 9^{a}	46 ± 8^{a,b}	48 ± 13^{b,c}	33 ± 15^{a,c}	62 ± 9^{b}
	2	19 ± 9^{a}	38 ± 14^{b}	35 ± 12^{b}	44 ± 14^{b,c}	62 ± 11^{c}
Whole-body retention, minus GI (% *of dose*)*	1	25 ± 9^{a}	42 ± 7^{a,b}	45 ± 12^{b}	31 ± 14 ^{a,b}	51 ± 8^{b}
	2	18 ± 9^{a}	36 ± 13^{b}	34 ± 12^{b}	42 ± 14^{b}	55 ± 9^{b}
Percentage of the retained dose in the GI tract**	1	9 ± 4^{a}	9 ± 2^{a,b}	6 ± 1^{a}	8 ± 3^{a}	18 ± 2^{b}
	2	4 ± 3^{a,b}	5 ± 2^{a}	4 ± 2^{b}	4 ± 2^{a,b}	13 ± 0.3^{c}
Percentage of the retained dose in the GI tract that is in the duodenum*	1	No data	No data	No data	No data	No data
	2	8 ± 7^{a,b}	6 ± 6^{b}	11 ± 9^{a,b}	15 ± 10^{b}	9 ± 2^{a,b}
Percentage of the retained dose in the pancreas*	1	No data	No data	No data	No data	No data
	2	1.1 ± 0.9^{a,b}	0.6 ± 0.5^{a}	0.7 ± 0.6^{a}	1.8 ± 1.2^{b}	4.7 ± 0.2^{c}
Percentage of the retained dose in 200 μL of blood	1	12 ± 3^{a}	16 ± 1^{b}	12 ± 2^{a}	9 ± 2^{c}	2 ± 0.5^{d}
	2	8 ± 2^{a}	9 ± 1^{a}	9 ± 1^{a}	5 ± 1^{b}	2 ± 0.3^{c}
Percentage of the retained dose in the liver	1	9 ± 4^{a}	16 ± 1^{b}	15 ± 2^{b}	25 ± 7^{c}	30 ± 5^{c}
	2	11 ± 3^{a}	9 ± 2^{a}	19 ± 3^{b}	39 ± 18^{c}	35 ± 2^{c}
Percentage of the retained dose in the kidneys	1	3 ± 1^{a}	3 ± 0.4^{a}	3 ± 1^{a}	3 ± 1^{a}	4 ± 1^{a}
	2	2 ± 1^{a}	2 ± 1^{a}	2 ± 1^{a}	2 ± 1^{a}	3 ± 0.2^{b}
Percentage of the retained dose in the spleen	1	2 ± 1^{a,b}	1 ± 0.4^{a,b}	1 ± 0.4^{a}	1 ± 1 ^{a}	3 ± 1^{b}
	2	0.1 ± 0.3^{a}	0.1 ± 0.1^{a}	0.4 ± 0.4^{b}	0.2 ± 0.2^{a,b}	2.5 ± 0.3^{c}
Percentage of the retained dose in the remaining carcass	1	66 ± 6^{a}	55 ± 1^{b}	63 ± 2^{a}	53 ± 5^{b}	43 ± 2^{c}
	2	74 ± 5^{a}	73 ± 3^{a}	66 ± 4^{b}	48 ± 15^{c}	41 ± 2^{c}
Estimated percentage of the retained dose incorporated into red cells***	1	72 ± 22^{a}	80 ± 4^{a,b}	64 ± 6^{a,b}	50 ± 12^{b}	10 ± 2^{c}
	2	68 ± 17^{a}	75 ± 6^{a}	73 ± 7^{a}	45 ± 10^{b}	10 ± 3^{c}

NOTE. Radiolabeled iron absorption and distribution as measured 5 days after dosing by gavage. Male mice were maintained on an iron-deficient diet from 1 week before gavage until the end of the study. In Study 1, mice were 4–5 weeks old when started on the iron-deficient diet, and in Study 2, mice were 8–17 weeks old. In Study 1, N = 11 WT, 3 *Heph*$^{-/-}$, 7 *Cp*$^{-/-}$, 8 *Heph*$^{int/int}$*Cp*$^{-/-}$, and 3 *Heph*$^{-/-}$*Cp*$^{-/-}$ mice. In Study 2, N = 14 WT, 13 *Heph*$^{-/-}$, 20 *Cp*$^{-/-}$, 14 *Heph*$^{int/int}$*Cp*$^{-/-}$, and 3 *Heph*$^{-/-}$*Cp*$^{-/-}$ mice. Mean ± SD. Results for whole-body retention and whole-body retention minus GI were examined by analysis of variance followed by Tukey's post hoc test in GraphPad Prism, whereas results for other analyses were examined by Welch *t* test and corrected for multiple comparisons with FDR. Statistics for Studies 1 and 2 were calculated separately. Most spleen and pancreas sample measurements in non *Heph*$^{-/-}$*Cp*$^{-/-}$ genotypes were near or below the limit of detection. For each analysis (row), groups that share at least 1 superscript letter are not significantly different (FDR-adjusted *P* value >.05).

*In Study 1, the pancreas was not separated from the GI tract, so the percentage of the retained dose in the GI tract includes the pancreas in Study 1 and excludes it in Study 2.

**In Study 1, the duodenum (defined here as the first 5 cm of small intestine) was not separated from the rest of the GI tract, so data on duodenal retention are not available.

***The estimated percentage of the retained dose incorporated into red cells was calculated for each mouse by using the counts in 200 μL of blood. Each mouse was assumed to contain approximately 60 μL of blood for every gram body weight for these estimates. N = 6 *Cp*$^{-/-}$ for Study 1 because body weight was missing for 1 mouse.

duodenal gut segments (Figure 7*C*). Radioactive iron was administered for 30 minutes via a ligated segment in anesthetized 8-week-old WT, *Heph*$^{-/-}$, and *Heph*$^{-/-}$*Cp*$^{-/-}$ mice (N = 3 per group) 5 days after they had been put on an iron-deficient diet. The ligated segment was then excised, opened, and washed, and the radioactive iron remaining in the gut segment, the wash solutions, the liver, and the rest of the carcass was counted. No significant differences between any of the groups were observed in the fraction of the total dose retained in the washed duodenal gut segment (data not shown). In addition, no significant differences were found in the percentage of the total dose transferred from the gut segment to the rest of the body (liver and rest of the carcass combined; Figure 7*C*). However, *Heph*$^{-/-}$*Cp*$^{-/-}$ mice had a significantly greater fraction of this transferred iron in the liver (59% ± 13%) than WT mice (5% ± 3%, Figure 7*C*). Although the percentage of transferred iron in the liver was greater in all individual *Heph*$^{-/-}$ mice (28% ± 19%) than WT mice, the difference was not statistically significant. In a separate control experiment performed in the same way, duodenal iron absorption was compared in 8-week-old *Fpn1*$^{int/int}$ mice (N = 3) and WT (*Fpn1* floxed) littermates (N = 3). The *Fpn1*$^{int/int}$ mice were severely anemic on the basis of their similar appearance to additional littermates whose hematology was examined (data not shown). FPN1 is the only known iron exporter in the intestine; thus if the ligated gut experimental procedure is performed correctly, iron transfer into the body should be extremely low (Figure 7*D*). As expected, the percentage of the total dose transferred from the gut segment to the rest of the body was very low (4% ± 4%) and significantly lower than that of WT controls (25% ± 4%).

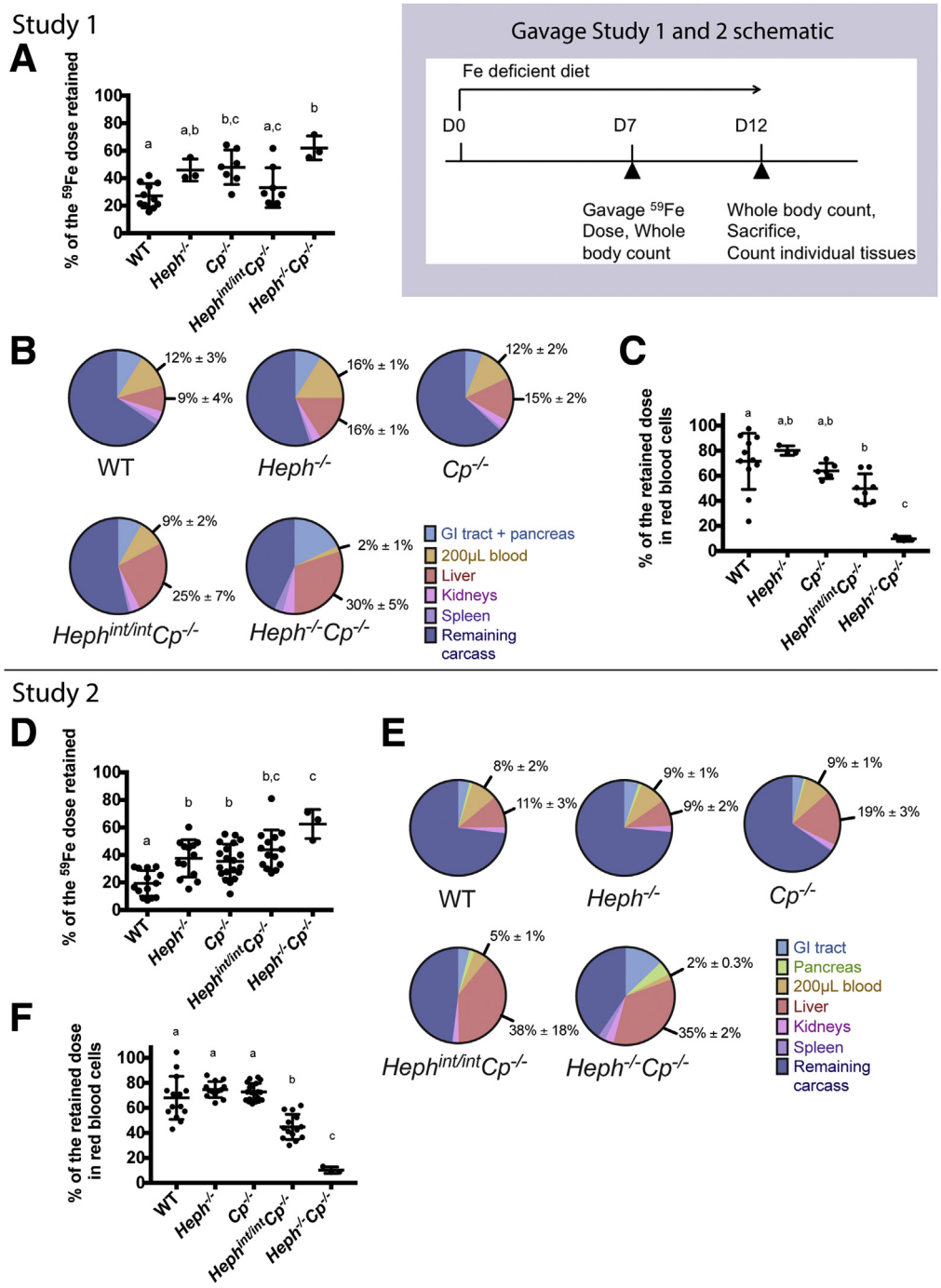

Figure 5. Intestinal iron absorption and iron distribution in young adult and adult male mice. *Top right:* design of Gavage Studies 1 and 2. On study day 0, male mice were changed from a standard rodent chow diet to an iron-deficient diet to stimulate intestinal iron absorption. One week later, mice were gavaged with a dose of radiolabeled iron, and whole-body radiation was measured. Five days later on study day 12, whole-body radiation was again measured, mice were euthanized, and tissues were collected. Radiation in the tissues was measured and used to quantify the amount of iron absorbed and how it was distributed. Mice in Gavage Study 1 were 4–5 weeks old, whereas those in Gavage Study 2 were 8–17 weeks old on study day 0. (*A–C*) Results from Gavage Study 1. (*D–F*) Results from Gavage Study 2. (*A* and *D*) Percent of the dose retained in the whole animal 5 days (typically sufficient time for complete turnover of the intestinal epithelium) after gavage is plotted for each genotype. (*B* and *E*) Distribution of the retained iron, expressed as the percentage in each tissue compartment (100 × (counts in tissue/sum of all counts for all tissues)). In Study 1, the pancreas was not excised from the GI tract and was thus counted as part of the GI tract. (*C* and *F*) The estimated percent of the retained dose incorporated into red cells as calculated for each mouse based on counts in 200 μL of blood. Each mouse was assumed to contain approximately 60 μL of blood for every gram body weight for these estimates. N = 6 $Cp^{-/-}$ for Study 1 because the body weight was missing for 1 mouse. Data are presented as mean and SD, and groups (panels *A*, *C*, *D*, and *F*) with at least 1 shared letter are not significantly different as determined by Welch *t* test corrected for multiple comparisons with FDR (FDR-adjusted *P* value >.05).

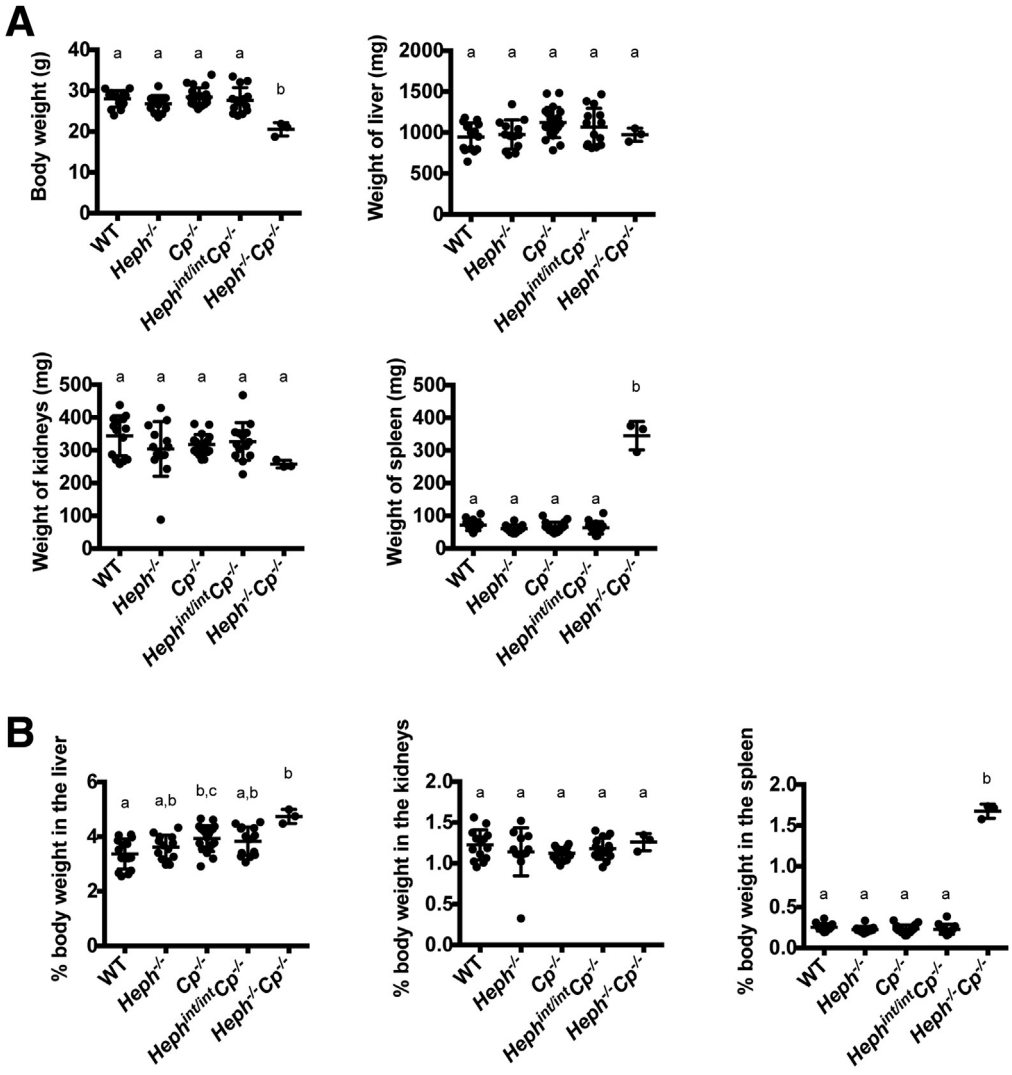

Figure 6. Body weight and relative liver, spleen, and kidney weights of animals in Gavage Study 2. (*A*) Whole-body weight and weight of individual tissues for each genotype. (*B*) Percent of total body weight in each tissue for each genotype. Data are presented as mean and SD. Groups with at least 1 shared letter are not significantly different as determined by Welch *t* test corrected for multiple comparisons with FDR (FDR-adjusted *P* value $>$.05).

Ferroportin 1 Protein Expression Is Increased and Localized to the Basolateral Membrane in Heph$^{-/-}$Cp$^{-/-}$ Duodenal Enterocytes

FPN1 expression (normalized to actin) was approximately 3 times higher in isolated duodenal enterocytes from adult 10- to 12-week-old male *Heph*$^{-/-}$ and *Heph*$^{-/-}$*Cp*$^{-/-}$ mice than it was in WT or *Cp*$^{-/-}$ mice, which had similar levels (Figure 8*A* and *B*). Immunofluorescence indicated a primarily basolateral localization of FPN1 in duodenal enterocytes of all genotypes examined, with greater expression at the villus tips. In agreement with the immunoblot results, signal intensity was greater in the *Heph*$^{-/-}$ and *Heph*$^{-/-}$*Cp*$^{-/-}$ villi than in the WT or *Cp*$^{-/-}$ villi. In addition, FPN1 was observed in cells in the lamina propria of *Heph*$^{-/-}$ and *Heph*$^{-/-}$*Cp*$^{-/-}$ mice but not in WT or *Cp*$^{-/-}$ mice (Figures 8*C* and 9).

Discussion

Both *Heph*$^{-/-}$*Cp*$^{-/-}$ and *Heph*$^{int/int}$*Cp*$^{-/-}$ mice were viable and able to absorb dietary iron, demonstrating that HEPH and CP are not absolutely required for intestinal iron absorption. However, study of these mice revealed that HEPH and CP together are critical for maintaining normal iron homeostasis in both the intestine and other tissues.

Although *Heph*$^{-/-}$*Cp*$^{-/-}$ and *Heph*$^{int/int}$*Cp*$^{-/-}$ mice survived, both double knockout strains had a more severe phenotype than mice lacking HEPH or CP alone. We previously reported that *Heph*$^{-/-}$ and *Heph*$^{int/int}$ mice exhibit iron loading in duodenal enterocytes throughout life and have an anemia when young that improves with age.[7] Iron levels in the tissues of *Heph*$^{-/-}$ and *Heph*$^{int/int}$ mice (with the exception of duodenal enterocytes) were low, but the phenotype of the *Heph*$^{-/-}$ mice was more pronounced than in the mice with intestine-specific knockout, suggesting that HEPH may play important roles in tissues other than the intestine.[7] On the other hand, *Cp*$^{-/-}$ mice have been shown to exhibit progressive iron loading in the liver (hepatocytes and Kupffer cells) and spleen (macrophages) and to have a mild anemia that persists throughout life.[15,17] We did not observe iron loading by Perls' staining in Kupffer cells in any mice lacking CP, possibly because we used younger mice than previous

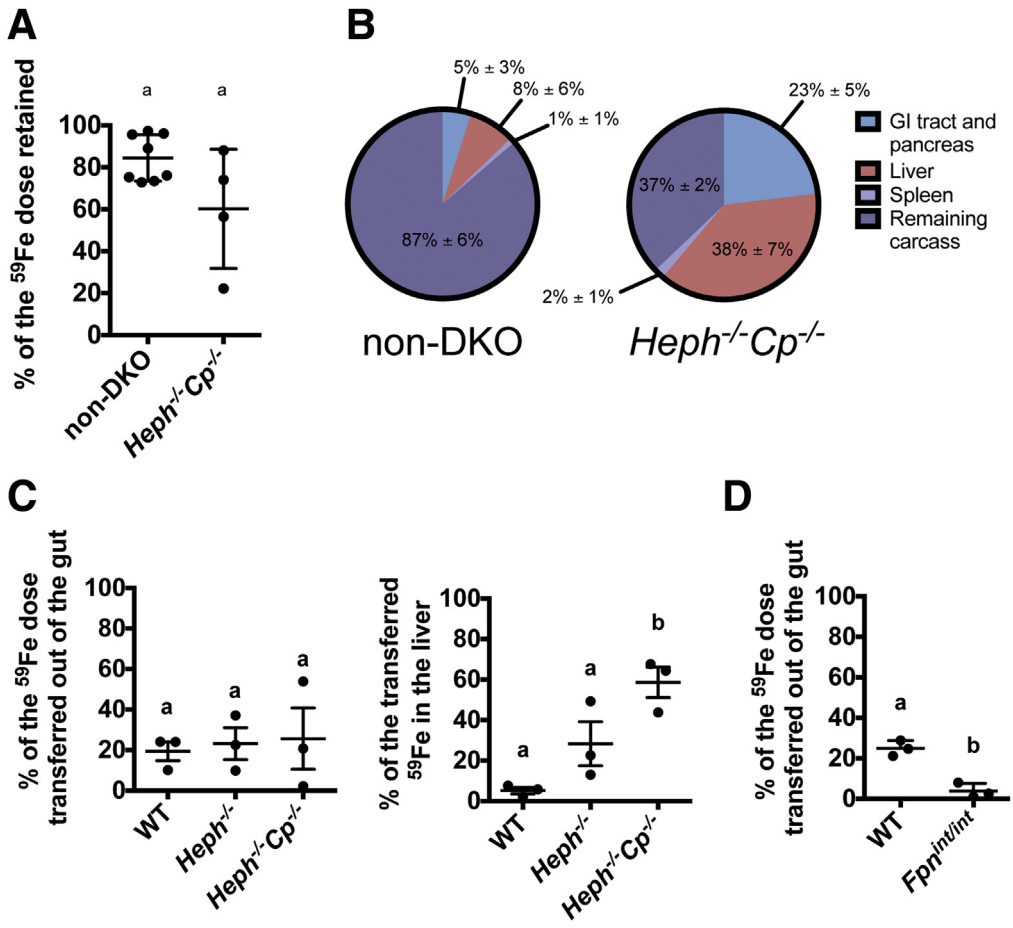

Figure 7. Intestinal iron absorption and iron distribution in suckling mice and in adult mice after absorption from a ligated duodenal segment. (*A*) Nursing 15-day-old male and female littermates were dosed by gavage with radiolabeled iron and then returned to their mother. The percent of the dose retained in the whole animals 4 days after gavage is plotted. (*B*) Distribution of the retained iron in (*A*), expressed as the percentage in each tissue compartment (100 × (counts in tissue/sum of all counts for all tissues)). For this experiment, the blood and the kidneys were not removed and were thus counted as part of the remaining carcass. Similarly, the pancreas was not excised from the GI tract and was thus counted as part of the GI tract. (*C*) A dose of radioactive iron was administered for 30 minutes via a ligated duodenal gut segment in anesthetized 8-week-old mice (N = 3 per group) 5 days after they had been put on an iron-deficient diet. The ligated gut segment was then excised, followed by the liver. The fraction of the dose transferred out of the gut segment was calculated as the sum of the counts in the liver and remaining carcass divided by the sum of the total counts in these tissues as well as in the excised ligated gut segment. The fraction in the liver was calculated as the counts in the liver divided by the sum of the counts in the liver and remaining carcass (not including the excised ligated gut segment). (*D*) In a similar experiment, control *Fpn1*$^{int/int}$ mice, which lack the iron transport protein required for basolateral iron export from enterocytes, showed negligible iron transfer from the ligated segment into the body, as expected. For each panel, the mean and SD are shown for each group. Groups with at least 1 shared letter are not significantly different as determined by Student *t* test (*P* value >.05) or Welch *t* test corrected for multiple comparisons with FDR (FDR-adjusted *P* value >.05).

studies.[17,18] In addition, but not studied here, the HEPH mutant strain *Heph*$^{sla/sla}$, *Heph*$^{-/-}$, and *Cp*$^{-/-}$ mice have all been reported to have disordered iron metabolism in the brain.[19–21]

Here we show that, similar to *Heph*$^{-/-}$ and *Heph*$^{int/int}$ mice, *Heph*$^{int/int}$*Cp*$^{-/-}$ mice had iron loading in the absorptive epithelial cells of the duodenum, suggesting reduced basolateral export of iron, and very little observable iron in the spleen by Perls' staining, suggesting systemic iron deficiency. However, unlike *Heph*$^{-/-}$ and *Heph*$^{int/int}$ mice but consistent with *Cp*$^{-/-}$ mice, liver non-heme iron levels were significantly greater in *Heph*$^{int/int}$*Cp*$^{-/-}$ mice than WT controls. The hematologic parameters of *Heph*$^{int/int}$*Cp*$^{-/-}$ mice suggested that they generally had less iron available for erythropoiesis than *Heph*$^{-/-}$, *Cp*$^{-/-}$, and WT controls. Male *Heph*$^{int/int}$*Cp*$^{-/-}$ mice were not statistically different from *Cp*$^{-/-}$ mice in any blood parameters, but they showed a trend toward a more anemic phenotype than *Cp*$^{-/-}$ mice.

Heph$^{-/-}$*Cp*$^{-/-}$ mice had a much more severe phenotype than *Heph*$^{int/int}$*Cp*$^{-/-}$ mice that was more complex than could be explained by the simple additive effect of the phenotypes of *Heph*$^{-/-}$ and *Cp*$^{-/-}$ mice. In addition to phenotypes observed in the *Heph*$^{int/int}$*Cp*$^{-/-}$ mice, including iron loading

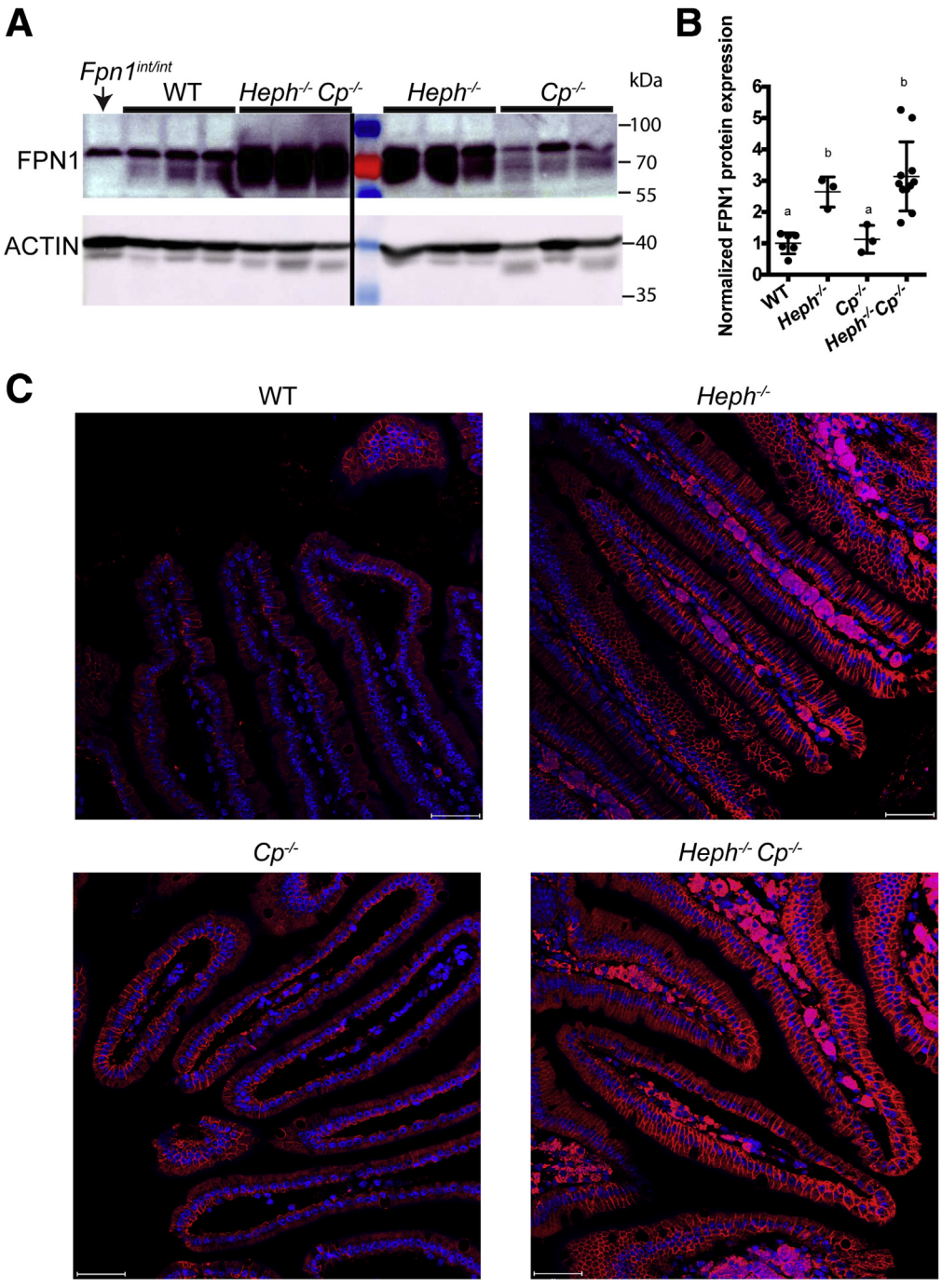

Figure 8. FPN1 expression and localization in knockout mouse models. (*A*) FPN1 expression was examined by immunoblotting of isolated duodenal enterocyte lysates from adult 10- to 12-week-old male WT, *Heph*$^{-/-}$, *Cp*$^{-/-}$, and *Heph*$^{-/-}$*Cp*$^{-/-}$ mice (N = 3 mice per genotype as shown). Duodenal enterocyte lysate from a 15-week-old *Fpn1*$^{int/int}$ mouse was used as a negative control for the FPN1 antibody (*lane 1*). The FPN1 antibody used here gives a non-specific band just above the *red ladder marker*. The lane just before the ladder representing a different genotype was removed using Adobe Photoshop (a *black vertical line* denotes where this lane was cut out). (*B*) Densitometry as performed on the immunoblot shown in (*A*) as well as an additional immunoblot with lysates from 3 additional WT and 8 additional *Heph*$^{-/-}$*Cp*$^{-/-}$ mice, for a total of 6 WT, 3 *Heph*$^{-/-}$, 3 *Cp*$^{-/-}$, and 11 *Heph*$^{-/-}$*Cp*$^{-/-}$ mice. FPN1 density was normalized to actin density in each lane, and then all results were normalized to the WT control group average. Mean and SD are shown. Groups with at least 1 shared letter are not significantly different as determined by Welch *t* test corrected for multiple comparisons with FDR (FDR-adjusted *P* value >.05). (*C*) FPN1 protein in formalin-fixed paraffin-embedded sections of proximal duodenal villi from adult 10- to 12-week-old male WT, *Heph*$^{-/-}$, *Cp*$^{-/-}$, and *Heph*$^{-/-}$*Cp*$^{-/-}$ mice was detected by immunofluorescence. FPN1 is stained *red,* and DAPI stained nuclei are in *blue*. Duodena from 4 WT mice, 5 *Heph*$^{-/-}$, 6 *Cp*$^{-/-}$, and 3 *Heph*$^{-/-}$*Cp*$^{-/-}$ mice were examined, and representative images are shown (original ×20 magnification with 50 μm scale bars). Images are a composite from the *red and blue channels*.

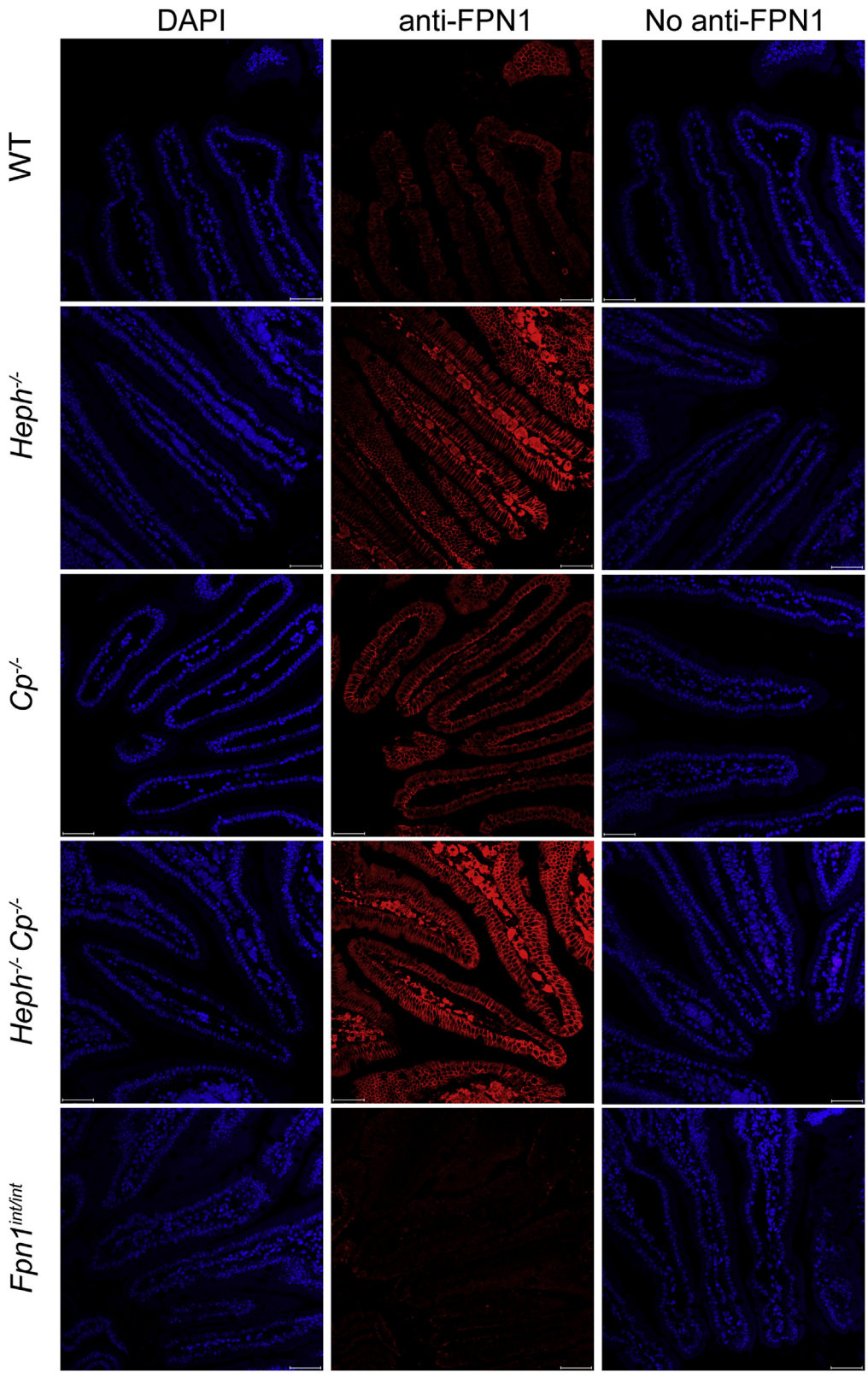

Figure 9. FPN1 immunofluorescence control images. *Blue* (DAPI) and *red* (anti-FPN1) single channel images (that were shown merged in Figure 8) are shown here for WT, *Heph*$^{-/-}$, *Cp*$^{-/-}$, and *Heph*$^{-/-}$*Cp*$^{-/-}$ genotypes, as well as from a *Fpn1*$^{int/int}$ control mouse. In the *last column*, representative composite *red and blue channel images* taken from slides treated only with DAPI and secondary antibody and no anti-FPN1 are shown. Original ×20 magnification, 50 μm scale bars.

in duodenal absorptive epithelial cells and the liver and lack of iron deposits in the spleen, *Heph*$^{-/-}$*Cp*$^{-/-}$ mice also exhibited a very severe anemia and marked iron loading in some peripheral tissues, including the pancreas, heart, adrenal glands, and, as also reported by collaborators, the kidneys and eyes.[22,23] The iron loading in the peripheral

tissues increased with age, but the anemia did not improve, suggesting that *Heph*$^{-/-}$*Cp*$^{-/-}$ mice were still able to obtain iron from the diet but that it was inappropriately distributed. Liver *Hamp1* expression was low in *Heph*$^{-/-}$*Cp*$^{-/-}$ mice, but despite their much more severe anemia and lower serum iron, it was not as low as in *Heph*$^{-/-}$ mice. This may be due to the high liver iron levels in *Heph*$^{-/-}$*Cp*$^{-/-}$ mice partially overcoming the suppression of hepcidin production. *Heph*$^{-/-}$*Cp*$^{-/-}$ mice also had white teeth throughout life (dark yellow-brown in WT littermates), possibly because of an iron transport defect in the enamel organ.[24] *Heph*$^{-/-}$*Cp*$^{-/-}$ mice, but not *Heph*$^{int/int}$*Cp*$^{-/-}$ mice, died prematurely, typically between 20 and 30 weeks of age, of unknown cause. Mice carrying the *sla* mutation in HEPH on a CP knockout background (*Heph*$^{sla/sla}$*Cp*$^{-/-}$) have also been reported to have an iron loading phenotype similar to *Heph*$^{-/-}$*Cp*$^{-/-}$ mice, and developed neurologic abnormalities (including weakness and gait changes), and died prematurely.[14,25] *Heph*$^{sla/sla}$*Cp*$^{-/-}$ mice also developed iron loading in the eye and degeneration with similarities to age-related macular degeneration, although the iron loading in the eye was not as severe as in *Heph*$^{-/-}$*Cp*$^{-/-}$ mice, suggesting that the *Heph*$^{-/-}$*Cp*$^{-/-}$ phenotype may in general be more severe.[22,26,27]

In intestinal iron absorption experiments where mice were gavaged with a dose of radiolabeled iron and whole-body retention was measured 5 days later, *Heph*$^{-/-}$*Cp*$^{-/-}$ mice surprisingly retained similar or higher levels of iron than controls. Greater than 13% of the retained iron in *Heph*$^{-/-}$*Cp*$^{-/-}$ mice was in the GI tract, 2–3 times more than any other genotype. The average life span of duodenal enterocytes, including the period before complete enterocyte differentiation when dietary iron absorption by these cells is low, is generally reported to be less than 5 days in adult mice, so we did not expect to observe such high GI iron retention in *Heph*$^{-/-}$*Cp*$^{-/-}$ mice.[28] There was no significant difference in the percentage of total GI tract radiolabeled iron in the duodena of *Heph*$^{-/-}$*Cp*$^{-/-}$ mice compared with the other genotypes (Table 4), suggesting that the retention was not due to iron retention in Brunner's glands, which were shown by Perls' stain to be iron loaded in *Heph*$^{-/-}$*Cp*$^{-/-}$ mice and are only found in the duodenum, or due solely to retention in enterocytes that had not turned over at the end of our study period. However, cells further down the intestinal tract may have taken up retained radiolabeled iron from sloughed duodenal cells, and if enterocyte turnover was modestly delayed, this could increase the amount of iron remaining in the gut. The large intestine has some capacity to absorb iron, and iron deficiency and hypoxia have been shown to upregulate iron transport proteins there.[29] We did not observe iron retention in the large intestine by Perls' staining in animals fed chow diets, but this method is not as sensitive as measurements with radioactive iron. GI iron retention was also observed in juvenile *Heph*$^{-/-}$*Cp*$^{-/-}$ mice when whole-body and intestinal iron were measured 4 days after dosing.

After subtracting the iron that was retained in the GI tract of both juvenile and adult *Heph*$^{-/-}$*Cp*$^{-/-}$ mice, approximately 50% of the total dose was absorbed by these mice, indicating that *Heph*$^{-/-}$*Cp*$^{-/-}$ mice can still absorb significant amounts of iron. Because intestinal iron absorption depends on both the ability of an animal to absorb iron (which is impaired in the absence of HEPH) as well as the drive to absorb iron (which is increased because of the severe anemia) and these processes are interdependent and involve many factors, it is difficult to compare iron absorption in mouse strains that show variation in each of these parameters. Although we did not directly compare iron absorption in *Heph*$^{-/-}$*Cp*$^{-/-}$ mice with that of WT mice made similarly severely anemic by prolonged feeding of an iron-deficient diet, we have previously shown that intestinal iron absorption in severely iron-deficient WT mice is typically >70%, with negligible iron retained in the GI tract.[7,30] This suggests that intestinal iron absorption in *Heph*$^{-/-}$*Cp*$^{-/-}$ mice, while still appreciable, is inappropriately low given their low hepcidin expression and severe anemia.

In Gavage Studies 1 and 2, *Heph*$^{-/-}$ mice also surprisingly absorbed more radiolabeled iron than WT mice, even when accounting for iron retained in the GI tract (~40% of the total dose, Table 4). The systemic iron deficiency and anemia in *Heph*$^{-/-}$ mice before being started on the iron-deficient study diet would be expected to increase their drive for intestinal iron absorption over that of WT mice, which have no block to iron absorption. Thus, *Heph*$^{-/-}$ mice likely had a higher drive for iron absorption than WT mice and may have absorbed more of the iron dose (but less in relation to their need and drive). In our previously published results (with WT and *Heph*$^{-/-}$ mice of similar age as those in Gavage Study 2 and under very similar conditions), we observed decreased whole-body iron dose retention in *Heph*$^{-/-}$ mice versus WT controls (*Heph*$^{-/-}$ = 32% ± 9%; WT = 54% ± 13%).[7] Although intestinal iron absorption by the *Heph*$^{-/-}$ mice in both studies was similar, absorption by the WT mice was nearly 3 times higher in this previously published study than in Gavage Study 2 (Table 4: *Heph*$^{-/-}$ = 38% ± 14%; WT = 19% ± 9%). It is thus possible that intestinal iron absorption was more stimulated in the WT mice in the previous study for unknown reasons that could include differences in the chow diet before the mice were put on the study diet or that mice in the previous study were fasted before dosing.

Although *Heph*$^{int/int}$*Cp*$^{-/-}$ and *Heph*$^{-/-}$*Cp*$^{-/-}$ mice were clearly still able to absorb iron, they exhibited perturbed systemic distribution of the iron. In both genotypes, a significantly larger proportion of the absorbed radiolabeled iron dose was found in the liver, and significantly less was incorporated into red cells, than in WT controls 5 days after dosing. This finding alone is not surprising because CP is required for normal rates of iron release from the liver, and *Cp*$^{-/-}$ mice also had a greater proportion of the iron dose in the liver than WT mice.[31] However, the *Heph*$^{-/-}$*Cp*$^{-/-}$ mice, and even more interestingly, *Heph*$^{int/int}$*Cp*$^{-/-}$ mice, had statistically greater retention of the absorbed iron dose in the liver than *Cp*$^{-/-}$ mice, suggesting that ablation of HEPH in intestinal enterocytes can also affect dietary iron retention by the liver. Lending some support to this, a significantly greater proportion of the retained

iron dose was located in the liver of *Heph*$^{-/-}$ mice than WT controls in Gavage Study 1.

In addition, distribution defects were observed in the 30-minute duodenal gut loop absorption experiment with *Heph*$^{-/-}$, *Heph*$^{-/-}$*Cp*$^{-/-}$, and WT control mice. A significantly greater proportion of the absorbed iron dose was found in the livers of *Heph*$^{-/-}$*Cp*$^{-/-}$ mice than in the livers of WT controls. *Heph*$^{-/-}$ mice also had a greater fraction of the absorbed iron dose in the liver in this experiment than WT mice, but the difference was not statistically significant, possibly because of the small number of mice examined. Steady-state non-heme iron levels in the livers of *Heph*$^{-/-}$ and *Heph*$^{int/int}$ mice, as measured by colorimetric assay here and previously, were significantly lower than in WT controls, making it likely that any extra iron absorbed or retained by the liver of mice just lacking HEPH is ultimately redistributed to the rest of the body, but perhaps over a longer time scale than tested in the gavage and gut loop experiments.[7] In contrast, *Cp*$^{-/-}$, *Heph*$^{int/int}$*Cp*$^{-/-}$, and *Heph*$^{-/-}$*Cp*$^{-/-}$ mice had higher steady-state levels of liver non-heme iron than WT mice.

One potential explanation for these perturbed iron distribution observations is that ablation of HEPH in duodenal enterocytes may prevent all or at least a fraction of the iron exported from the intestine from binding to TF. As a result, this iron would enter the portal vein as non-transferrin bound iron (NTBI). Because the duodenal circulation travels first to the liver before joining the general circulation, this iron would be rapidly taken up by the liver, which has a particularly high affinity for NTBI, as demonstrated in studies of intestinal iron absorption in mice either lacking TF or with fully saturated TF.[32] Eventually, however, this iron would be released from the liver to be redistributed to other tissues. In mice with ablation of CP as well, the rate of iron release from the liver would be decreased, leading to increased clearance times for iron and increased steady-state levels of liver iron.

Overall, the peripheral tissue iron loading and the severe anemia phenotype of *Heph*$^{-/-}$*Cp*$^{-/-}$ mice, especially in contrast to the phenotype of *Heph*$^{int/int}$*Cp*$^{-/-}$ mice, indicate an important role for extra-intestinal HEPH in systemic iron metabolism that becomes critical in the absence of CP. Osaki et al[33,34] proposed 2 mechanisms (later supported by evidence) by which CP could facilitate erythropoiesis: increasing iron binding to TF, and increasing iron release from stores, and both of these could apply as well to extra-intestinal HEPH.[13,15] Because erythropoiesis is almost entirely dependent on TF-bound iron, any impairment in the delivery of iron to TF when HEPH is ablated could exacerbate anemia. A potential parallel may be seen in the hypotransferrinemic mouse.[35] With little or no functional TF, these mice develop a severe anemia, and circulating NTBI is rapidly cleared by the liver and other peripheral tissues, giving a pattern of iron loading similar to that of *Heph*$^{-/-}$*Cp*$^{-/-}$ mice. However, the spleen in both models is spared, and hepcidin levels remain neglible.[35,36] Direct impairment of iron efflux from extra-intestinal cells could also be a cause of the severe anemia and the peripheral iron loading observed in *Heph*$^{-/-}$*Cp*$^{-/-}$ mice. As has been reported for CP, HEPH may maintain the rate of iron efflux from some cell types by decreasing FPN1 turnover.[10] However, at least in duodenal enterocytes, mice lacking HEPH (as shown previously) or lacking both HEPH and CP exhibited increased FPN1 protein expression that appeared to be properly localized, suggesting that lack of FPN1 is not responsible for the iron loading in duodenal enterocytes.[7] More detailed studies are needed to decipher the cause of the severe anemia and tissue iron loading in the *Heph*$^{-/-}$*Cp*$^{-/-}$ mice and to determine which cell types are involved.

In summary, intestinal iron absorption can occur in mice lacking HEPH and CP, but both proteins are required for the proper systemic distribution of the absorbed iron. Systemic lack of both proteins leads to a severe anemia coupled with marked iron overload in various other tissues, leading to premature death in adulthood. Our results confirm the importance of HEPH in extra-intestinal tissues for maintaining whole-body iron metabolism, and they suggest that lack of HEPH and CP leads to increased NTBI.

Materials and Methods

Ethics Statement

All work performed was in accordance with the National Institutes of Health (NIH) guidelines, as described in the Guide for the Care and Use of Laboratory Animals of the NIH, and with approval from the Office of Laboratory Animal Care at the University of California, Berkeley, and the QIMR Berghofer Medical Research Institute Animal Ethics Committee. In vivo experiments are reported here in accordance with the ARRIVE guidelines.[37] All efforts were made to minimize animal suffering. All authors had access to the study data and have reviewed and approved the final manuscript.

Mouse Models

Mice null for both HEPH and CP (*Heph*$^{-/-}$*Cp*$^{-/-}$), as well as WT and single knockout mice for these genes, were generated from crosses of *Heph*$^{-/-}$ mice, *Cp*$^{-/-}$ mice, and their progeny. The generation and phenotypes of the 2 single knockout strains have been previously described.[7,17] *Heph* is located on the X chromosome, but for simplicity, female as well as male mice hemizygous for the *Heph* knockout allele are designated as *Heph*$^{-/-}$. Pups from *Heph*$^{+/-}$*Cp*$^{+/-}$, *Heph*$^{+/-}$*Cp*$^{-/-}$, and *Heph*$^{+/-}$ females bred with WT, *Heph*$^{-/-}$, *Heph*$^{-/-}$*Cp*$^{-/-}$, *Cp*$^{+/-}$ and *Cp*$^{-/-}$ males were used in these studies. Females with homozygous knockout of HEPH were not used as breeders because their pups are iron deficient regardless of pup genotype.

Mice with whole-body knockout of CP but deletion of HEPH only in the intestine (*Heph*$^{int/int}$*Cp*$^{-/-}$) were generated from crosses of *Heph*$^{int/int}$ mice, *Cp*$^{-/-}$ mice, and their progeny. *Heph*$^{int/int}$ mice are HEPH floxed (C57BL/6-Heph$^{tm1.1Jdun}$, referred to here as *Heph*$^{fl/fl}$) mice bearing 1 copy of the villin-cre transgene Tg(Vil-cre)997Gum and have been previously described.[7] These mice carry floxed alleles of *Heph* and 1 copy of the villin-cre transgene. For these studies, we used *Heph*$^{int/int}$*Cp*$^{-/-}$ and their *Heph*$^{fl/fl}$*Cp*$^{-/-}$ littermates lacking the villin-cre transgene that were generated

by crossing $Heph^{fl/fl}Cp^{-/-}$ females with $Heph^{int/int}Cp^{-/-}$ males. $Heph^{fl/fl}Cp^{-/-}$ mice lacking the villin-cre transgene are phenotypically $Cp^{-/-}$, and we included them in our studies as part of the $Cp^{-/-}$ group.

Tamoxifen-induced FPN1 intestinal knockout mice ($Fpn1^{int/int}$) were generated as previously described after several crosses of *Fpn1* floxed mice on a mixed C57BL/6J and 129/SvEvTac background (provided by Professor Nancy Andrews at Duke University) with mice bearing the villin-creERT2 transgene Tg(Vil-Cre/ERT2)23Syr and injection with tamoxifen.[7,8,38] Mice for all studies were on the C57BL/6J background unless otherwise noted.

Animal Husbandry

Mice were maintained on a standard rodent chow diet containing approximately 160 mg/kg iron (Norco Stockfeeds, South Lismore, NSW, Australia) or, for intestinal iron absorption studies as indicated, an iron-deficient diet made in-house as described previously.[39] Mice fed the iron-deficient diet and dosed with ^{59}Fe were provided with deionized water and housed in grid-bottom cages designed to minimize coprophagia. For some studies where a control group with iron deficiency anemia was required, mice were weaned onto the iron-deficient diet and maintained on the diet until they were studied. All mice were allowed unlimited access to food and water.

Tissue Collection

Mice were euthanized by CO_2 gas inhalation or anesthetized by a single intraperitoneal injection of 44 mg/kg ketamine and 8 mg/kg xylazine in saline. Blood was then collected from the posterior vena cava and heart. For each mouse, approximately 250 μL of blood was collected into potassium ethylenediaminetetraacetic acid tubes (Terumo Corporation, Tokyo, Japan; cat #3T-MQK) for whole blood analysis or into 1.5 mL microfuge tubes without anticoagulant to provide serum. Tissues were harvested, trimmed to remove connective tissue, and either immediately snap frozen in liquid nitrogen for future RNA/protein analyses or incubated in 10% phosphate-buffered formalin overnight at 25°C for future paraffin embedding. Enterocytes were collected as previously described.[7] For serum samples, blood was allowed to clot, centrifuged to pellet cells, and then the serum was removed. An additional centrifugation step was then performed to ensure all cells were removed, and then the serum was snap frozen.

Polymerase Chain Reaction Genotyping

Mice were routinely genotyped by polymerase chain reaction (PCR) using DNA obtained from a 1- to 2-mm piece of the distal tail tip or from a small ear punch sample as described previously.[7] Primers, annealing temperatures, and expected product sizes are described in Table 5.

Protein and RNA Analyses

A small frozen piece of each tissue was removed from low temperature storage and disrupted by vigorous shaking with 1.4-mm ceramic beads as described previously.[7] For RNA preparation, this homogenization step was performed in ice-cold TRIzol (Invitrogen, Melbourne, VIC, Australia), and RNA was extracted as per the manufacturer's instructions. Complementary DNA was synthesized by using oligo(dT) primers and Moloney Murine Leukemia Virus reverse transcriptase (Invitrogen) as per the manufacturer's instructions. Real-time quantitative PCR was performed by using the LightCycler 480 SYBR Green I Master Mix in an LC480 machine (Roche, Basel, Switzerland) as per the manufacturer's instructions, and the data were analyzed by calculating the concentration of each sample from its Ct value by using a standard curve made from pooled sample complementary DNA as described previously.[40] The results were then normalized to the expression of the housekeeping gene hypoxanthine guanine phosphoribosyltransferase (*Hprt*). All primers (Table 5) were previously validated by melt-curve analysis, PCR product size analysis, and PCR product sequencing.

For protein expression analysis by immunoblotting, tissue was homogenized in ice-cold lysis buffer (25 mmol/L Tris-HCl, pH 7.2, 25 mmol/L NaCl, 0.25% Tween-20, 0.25% NP-40, 0.1% sodium dodecyl sulfate) with protease inhibitors as per the manufacturer's instructions (Complete protease inhibitor cocktail tablets, Roche; cat #11697498001). The homogenized sample was centrifuged at 16,000*g* for 30 minutes at 4°C to pellet debris, and the supernatant was then collected and assayed for protein concentration by using the Pierce BCA Protein Assay Kit (Thermo Fisher Scientific, Rockford, IL). Total protein (60–80 μg) was mixed with sodium dodecyl sulfate loading buffer with fresh dithiothreitol. The samples were separated on 10% Tris-glycine sodium dodecyl sulfate polyacrylamide denaturing gels and then transferred to Immobilon-FL polyvinyl difluoride membranes (Merck, Kilsyth, Australia). Membranes were blocked for 1 hour at room temperature with shaking in blocking buffer (10% non-fat milk in Tris-buffered saline with 0.1% Tween-20 [TBST]). Membranes were then incubated with the relevant primary antibody (mouse monoclonal anti-beta actin antibody, 1:10,000 dilution, cat #ab6276; Abcam, Cambridge, UK, or rabbit polyclonal anti-FPN1 antibody EB9[41,42], 1:500 dilution) diluted in blocking buffer for 1 hour at room temperature. The membranes were then washed with TBST and incubated for 1 hour at room temperature with secondary antibody (goat anti-rabbit horseradish peroxidase, 1:8000 dilution; Invitrogen, cat #65-6120, or goat anti-mouse horseradish peroxidase, 1:10,000 dilution; Invitrogen, cat #62-6520). The blots were washed in TBST and imaged on film or in a digital imager (LAS500; GE Healthcare, Little Chalfont, United Kingdom) after incubation with the Western Lightning Plus-ECL Kit solutions (Perkin-Elmer, Glen Waverley, VIC, Australia). Densitometry was performed by using the TotalLab Quant software (Newcastle upon Tyne, United Kingdom). For each sample, results for the protein of interest were normalized to that of actin. The results for each mouse group were then averaged and normalized to the average result for the WT control group for data presentation.

Table 5. Primers

Gene	Primer Name	Primer sequence	Anneal Temperature (°C)	Expected products
Heph (WT and floxed alleles) genotyping	DL1 DL2	5′- GACCTAGGAAGGAGAATCATGAG -3′ 5′- TTTGCGAGCCGACCTTACACC -3′	55	240 bp = WT allele present; 300 bp = *Heph* floxed allele present
Heph (knockout allele) genotyping	KO1 KO2 oIMR7338* oIMR7339*	5′- TGTCATTCAATTCCTGGAAAA -3′ 5′- CCAAGAAAATGGAGAAAGAGG -3′ 5′- CTAGGCCACAGAATTGAAAGATCT -3′ 5′- GTAGGTGGAAATTCTAGCATCATCC-3′	55	320 bp = reaction successful; 230 bp = *Heph* knockout allele present
Villin-cre recombinase transgene genotyping	oIMR1878* oIMR1879* oIMR0015* oIMR0016*	5′- GTGTGGGACAGAGAACAAACC -3′ 5′- ACATCTTCAGGTTCTGCGGG -3′ 5′- CAAATGTTGCTTGTCTGGTG -3′ 5′- GTCAGTCGAGTGCACAGTTT -3′	64	200 bp = reaction successful; 1100 bp = villin-cre transgene present
Cp (WT allele) genotyping	oIMR1117* oIMR1118*	5′- CATACTCTGAACACCCTGAGAAAG -3′ 5′- CATCAGATACCAGTTGACTTCATC -3′	58	500 bp band = *Cp* WT allele present
Cp (knockout allele) genotyping	oIMR1117* oIMR1119*	5′- CATACTCTGAACACCCTGAGAAAG -3′ 5′- CCCGTGATATTGCTGAAGAGCTTG -3′	64	1000 bp band = *Cp* knockout allele present
Villin-creERT2 cre recombinase genoytping	vERT2-Cre 198 vERT2-2kbseqS	5′- CGCGAACATCTTCAGGTTCT -3′ 5′- CAAGCCTGGCTCGACGGCC -3′	55	260 bp = Villin-creERT2 transgene present
Hamp1 (real-time qPCR)	Hamp1F Hamp1R	5′- AGAGCTGCAGCCTTTGCAC -3′ 5′- ACACTGGGAATTGTTACAGCATTTA -3′	58	130 bp product
Hprt (real-time qPCR)	HprtF HprtR	5′- GGACTGATTATGGACAGGA -3′ 5′- GAGGGCCACAATGTGATG -3′	58	78 bp product

NOTE. The sequences of the starred (*) primers are from The Jackson Laboratory website, www.jax.org.
bp, base pair; qPCR, quantitative PCR.

Tissue Iron Staining and Quantitative Tissue Iron Measurements

Paraffin-blocked tissues were sectioned and stained for ferric iron using Perls' Prussian blue stain with or without enhancement with DAB by the Histotechnology Facility at QIMR Berghofer.[43] In brief, tissues were submitted to the Facility in 70% ethanol after overnight incubation at room temperature in phosphate-buffered saline (PBS) solution with 10% formalin. Tissues were dehydrated in ethanol, cleared with xylene, and then embedded in paraffin. Sections 4 μm in thickness were cut, mounted on slides, and then deparaffinized. After rehydration in deionized water, the sections were incubated for 15–30 minutes in an equal volume mixture of 4% hydrochloric acid (HCl) and freshly prepared 4% aqueous potassium ferrocyanide. Sections were washed in distilled water and then counterstained with nuclear fast red for 10 minutes. The slides were then washed, dehydrated, and mounted. Slides were scanned using an Aperio ScanScope (Leica Biosystems, Wetzlar, Germany) AT2 light microscope on the $\times$40 magnification setting. For colorimetric non-heme iron quantification, a modification of the Torrance and Bothwell method was used as described previously.[7]

Immunofluorescence

Tissue sections (4 μm) were cut from paraffin-blocked duodena and mounted on glass slides, dewaxed with xylene, and then rehydrated with a series of alcohols. For antigen retrieval, sections were incubated in 10 mmol/L citrate buffer pH 6.0 containing 0.05% Tween-20, heated to boiling, and maintained at 95°C for 20 minutes. Sections were then incubated in 50 mmol/L glycine/NH_4Cl for 15 minutes at room temperature to prevent endogenous fluorescence, blocked for 1 hour at room temperature with 10% fluorescence dilution buffer (1 mmol/L $CaCl_2$, 1 mmol/L $MgCl_2$, 5% goat serum, 5% fetal bovine serum, 2% bovine serum albumin, PBS), and incubated with FPN1 rabbit polyclonal primary antibody EB9 (1/500 dilution) overnight at 4°C. Subsequent to washing with PBS, the sections were incubated with secondary antibody (Molecular Probes goat anti-rabbit Alexa Fluor A594; Life Technologies, Carlsbad, CA; cat #A-11012, 1/500 dilution) for 30 minutes, washed with PBS, and incubated with DAPI counterstain for 5 minutes at room temperature. After further PBS washes, the sections were mounted in Prolong Gold antifade mountant (Life Technologies). Sections were viewed with a Zeiss LSM780 with AxioObserver confocal microscope with a Plan-Apochromat $\times$20/0.8 M27 objective, and images were acquired and analyzed using the Zeiss Zen software.

Blood Analyses

The anticoagulated blood samples in ethylenediaminetetraacetic acid were analyzed at the Pathology Department of the Royal Brisbane and Women's Hospital (Brisbane, Australia) using a Sysmex XE-5000 automated hematology analyzer (Roche Diagnostics, Castle Hill, NSW, Australia). Serum iron, TIBC, and TF saturation were measured by using the ferrozine-based Iron/TIBC Reagent Set (Pointe Scientific Inc, Canton, MI). These assays were performed per the manufacturer's instructions, but they were scaled down linearly by a factor of 20 and performed in a 96-well plate, as previously described.[30] Analyses were performed on samples of serum that had undergone a single freeze-thaw cycle.

Intestinal Iron Absorption Assays

Intestinal iron absorption was studied either by dosing by gavage, as described previously, or by dosing via an isolated duodenal gut segment.[7] The mice were not fasted before or after the dosing to avoid additional stress on the *Heph*$^{-/-}$*Cp*$^{-/-}$ mice.

Gavage studies in young adult (Study 1) and adult (Study 2) mice. At a mean age of 5.6 $\pm$ 0.5 weeks (Study 1) or 13.1 $\pm$ 2.4 weeks (Study 2), male mice initially maintained on a chow diet were switched to an iron-deficient diet to stimulate iron absorption. After 1 week on the diet, the mice were dosed by gavage with 100 μL of a freshly prepared solution containing 200 μmol/L ferrous sulfate in 10 mmol/L HCl, spiked with $\sim$3 μCi ^{59}Fe as ferric chloride (Perkin-Elmer, Waltham, MA; cat #NEZ037001MC) per dose. In Study 1, the mice were dosed in 3 groups over 2 days in the 10:00 AM to 3:00 PM window. In Study 2, the mice were dosed in 4 groups over 2 days between 11:00 AM and 2:00 PM. The radiation in each mouse was measured by using a RAM DA gamma counter with a PM-11 tube (Rotem Industries, Arava, Israel) at a fixed distance just after dosing and then again 5 days later. By this time, any iron not absorbed by intestinal enterocytes should have cleared from the mouse, and there should be complete turnover of the intestinal epithelium. However, this period of time is not long enough for substantial iron excretion to occur. On the basis of the findings of Stevens et al[44] and our own data on biliary and urinary iron excretion (Lu et al, unpublished), we estimate total excretion to be no more than 2.5% of body iron during this period.[23] After subtraction of the background counts, the percentage of the initial dose remaining in each mouse was calculated.

Mice were then euthanized by ketamine/xylazine/saline as described above. They were then weighed, and the body cavity was opened on a small sheet of plastic-backed absorbent material (Benchkote; Whatman, Maidstone, United Kingdom). Blood was collected from the posterior vena cava, and 200 μL was immediately aliquoted into a separate tube. The GI tract, comprising the lower esophagus just proximal to the stomach down to the anus and including the pancreas, connective tissue, and any contents inside the GI tract, was then excised. In Study 2, but not in Study 1, the pancreas was cut away from the GI tract and wrapped in foil, and the first 5 cm of small intestine was excised from the GI tract and wrapped in a piece of foil, to later measure the radiolabeled iron in the pancreas and duodenum, respectively. The remaining GI tract was placed in a 10 mL tube. The spleen, liver, and kidneys were then excised from the carcass, weighed on a microscale, and wrapped in foil (1 tissue per foil packet). Any blood on the dissection instruments was wiped on the Benchkote. The

remaining carcass and syringe/needle/pipet tip used to collect blood were wrapped together in the Benchkote and placed in a 50 mL tube and labeled "remaining carcass". After clotting, the 200 μL blood samples from Study 2 were centrifuged to separate serum from the red cell pellet to later determine the radioactivity in each fraction separately. The spleen, liver, kidneys, pancreas, and duodenum were placed in an oven at 110°C and allowed to dry overnight, and the remaining carcass, GI tract, and the 200 μL blood sample (or separated serum and red cell samples, for Study 2) were frozen at –20°C. The next day, the radioactivity in the liver, kidney, spleen, pancreas, 200 μL blood, duodenum, GI tract, and remaining carcass was measured separately at a fixed distance from the gamma counter. After background subtraction, the percentage of radiation in each tissue relative to the total in the whole animal was calculated by dividing the counts in a particular tissue by the sum of counts in all the tissues and then multiplying by 100. Values near the limit of detection that were below 0 after background subtraction (primarily for the spleen) were assigned a value of 0.

In addition, an estimation of the proportion of radioactivity in each animal's total blood volume was calculated. The total blood volume of each mouse in microliters was first estimated by multiplying the weight of the mouse in grams by 60 (assuming approximately 60 μL blood per gram of mouse body weight).[16] The estimated total blood volume was then multiplied by the counts per microliter of blood (minus background) in the 200 μL blood sample. The estimated total counts in the blood were then divided by the total counts retained in the mouse (minus background), and then the result was multiplied by 100 to give the estimate of the percentage of the radioactivity in the blood.

Gavage study in suckling mice. Suckling mice were housed with their mothers, who were maintained on a chow diet. At 11 days of age, male and female juvenile littermates were gavaged together in 1 batch with radiolabeled iron, and the total dose was counted as described above. Four days after the gavage, the total dose retained was measured, and then the mice were euthanized by ketamine/xylazine/saline intraperitoneal injection as described under "Tissue collection". The liver, spleen, and GI tract, comprising the lower esophagus just proximal to the stomach down to the anus and including the pancreas, connective tissue, and any contents inside the GI tract, were excised. The radioactivity in the liver, spleen, GI tract, and remaining carcass was measured separately at a fixed distance from the gamma counter. After background subtraction, the percentage of radiation in each tissue relative to the total in the whole animal was calculated by dividing the counts in a particular tissue by the sum of counts in all the tissues and then multiplying by 100.

Isolated duodenal gut loop studies. In experiments where iron absorption was studied by dosing via an isolated duodenal gut loop, a procedure that has been previously described in experiments with rats was used and modified slightly for mice.[45] In brief, a mouse was placed in an induction chamber and anesthetized by inhalation of 2.5% isoflurane in oxygen, delivered at a flow rate of 2 L/min by using a veterinary anesthetic machine (The Stinger; Advanced Anaesthesia Specialists, Gladesville, NSW, Australia). The mouse was then removed from the chamber and placed ventral side up on a prewarmed (37°C) heating pad covered with 2 layers of Benchkote (one piece large enough to cover the whole heating pad and another piece on top just larger than the mouse). The nose and mouth of the mouse were immediately placed inside a nose cone that was connected to a continuous flow of 1 L/min oxygen with 1.5% isoflurane anesthetic. Mice were monitored throughout the whole experiment to ensure adequate depth of anesthesia.

After ensuring the mouse was unresponsive to paw pinch, a midline incision was made in the abdomen. The duodenum was exposed, and 3 loose ligatures were placed around it, with care taken to avoid positioning that could impair blood flow once the ligatures were tied. Two of the ligatures were placed approximately 0.5 cm distal to the pylorus and one at the ligament of Treitz. A small incision was made just proximal to the uppermost ligature, a cannula was inserted, and the upper ligature was tied to secure the cannula. A second incision was then made just distal to the lowest ligature. The duodenal segment was flushed with 5 mL saline solution (prewarmed to 37°C) via the cannula, and then the lower ligature was tightened. The duodenal segment was then infused with 100 μL of a freshly prepared solution containing 200 μmol/L ferrous sulfate in 10 mmol/L HCl and spiked with $\sim$3 μCi ^{59}Fe as ferric chloride (Perkin-Elmer; cat # NEZ037001MC) per dose. Next, the second ligature at the proximal end of the segment was tied off, and the cannula was removed. The abdomen of the animal was then covered with warm, damp gauze to prevent drying.

Thirty minutes after the iron dose was administered, the duodenal segment was carefully excised and placed on a separate small piece of Benchkote (the Benchkote piece was checked later by counting to ensure that the duodenal gut segment had not leaked). The animal was then euthanized by cervical dislocation. The duodenal segment was cut across at both ends and washed extensively with 20 mL saline. The wash solutions were recovered and saved for analysis. Any attached pancreas and mesentery were carefully trimmed from the exterior of the duodenal segment and placed on the Benchkote with the rest of the carcass. The duodenal segment was wrapped in a piece of foil. The whole liver was then excised from the carcass and wrapped in a separate piece of foil. The rest of the carcass was then wrapped in the Benchkote piece beneath it and placed in a 50 mL tube.

The radioactivity in the wash solution, the duodenal segment, the liver, and the remaining carcass was counted by using a RAM DA Gamma Counter with a PM-11 tube at a distance of 10 cm, and background was subtracted. The total ^{59}Fe dose (total counts) was calculated as the sum of the counts in the wash, gut segment, liver, and remaining carcass. The percentage of the total dose retained in the gut segment was calculated by dividing the counts in the gut segment by the total counts and multiplying by 100. The transferred dose was defined as the total number of counts in the liver and remaining carcass, ie, the iron that had been

transferred out of the gut segment to the rest of the body. The percentage of the transferred dose in the liver was calculated by dividing the counts in the liver by the sum of the counts in the liver and the remaining carcass and then multiplying by 100.

Statistics

All values are expressed as mean ± standard deviation (SD). For comparisons between 2 groups, Student *t* test and the F test for equal sample variance were performed in GraphPad Prism (Sunnyvale, CA) version 6.0c for Mac OS X. For comparisons among multiple groups, Welch *t* test followed by false discovery rate (FDR) correction for multiple comparisons was performed by using the stats package in R. We applied .05 as the cutoff for *P* values and FDR-adjusted *P* values; the null hypotheses were tested against two-sided alternatives and rejected if the *P* value or FDR-adjusted *P* value was less than .05.

References

1. Collins JF, Anderson GJ. Molecular mechanisms of intestinal iron transport. In: Johnson LR, ed. Physiology of the gastrointestinal tract. 5th ed, vol 1. Oxford: Academic Press, 2012:1921–1948.
2. Patel BN, David S. A novel glycosylphosphatidylinositol-anchored form of ceruloplasmin is expressed by mammalian astrocytes. J Biol Chem 1997;272:20185–20190.
3. Fortna RR, Watson HA, Nyquist SE. Glycosyl phosphatidylinositol-anchored ceruloplasmin is expressed by rat Sertoli cells and is concentrated in detergent-insoluble membrane fractions. Biol Reprod 1999;61:1042–1049.
4. Marques L, Auriac A, Willemetz A, Banha J, Silva B, Canonne-Hergaux F, Costa L. Immune cells and hepatocytes express glycosylphosphatidylinositol-anchored ceruloplasmin at their cell surface. Blood Cells Mol Dis 2012;48:110–120.
5. Vulpe CD, Kuo YM, Murphy TL, Cowley L, Askwith C, Libina N, Gitschier J, Anderson GJ. Hephaestin, a ceruloplasmin homologue implicated in intestinal iron transport, is defective in the sla mouse. Nat Genet 1999;21:195–199.
6. Chen H, Attieh ZK, Syed BA, Kuo YM, Stevens V, Fuqua BK, Andersen HS, Naylor CE, Evans RW, Gambling L, Danzeisen R, Bacouri-Haidar M, Usta J, Vulpe CD, McArdle HJ. Identification of zyklopen, a new member of the vertebrate multicopper ferroxidase family, and characterization in rodents and human cells. J Nutr 2010;140:1728–1735.
7. Fuqua BK, Lu Y, Darshan D, Frazer DM, Wilkins SJ, Wolkow N, Bell AG, Hsu J, Yu CC, Chen H, Dunaief JL, Anderson GJ, Vulpe CD. The multicopper ferroxidase hephaestin enhances intestinal iron absorption in mice. PloS One 2014;9:e98792.
8. Donovan A, Lima CA, Pinkus JL, Pinkus GS, Zon LI, Robine S, Andrews NC. The iron exporter ferroportin/Slc40a1 is essential for iron homeostasis. Cell Metab 2005;1:191–200.
9. Jeong SY, David S. Glycosylphosphatidylinositol-anchored ceruloplasmin is required for iron efflux from cells in the central nervous system. J Biol Chem 2003;278:27144–27148.
10. De Domenico I, Ward DM, di Patti MC, Jeong SY, David S, Musci G, Kaplan J. Ferroxidase activity is required for the stability of cell surface ferroportin in cells expressing GPI-ceruloplasmin. EMBO J 2007;26:2823–2831.
11. Kono S, Yoshida K, Tomosugi N, Terada T, Hamaya Y, Kanaoka S, Miyajima H. Biological effects of mutant ceruloplasmin on hepcidin-mediated internalization of ferroportin. Biochim Biophys Acta 2010;1802:968–975.
12. Potdar AA, Sarkar J, Das NK, Ghosh P, Gratzl M, Fox PL, Saidel GM. Computational modeling and analysis of iron release from macrophages. PLoS Computational Biology 2014;10:e1003701.
13. Cherukuri S, Potla R, Sarkar J, Nurko S, Harris ZL, Fox PL. Unexpected role of ceruloplasmin in intestinal iron absorption. Cell Metab 2005;2:309–319.
14. Xu X, Pin S, Gathinji M, Fuchs R, Harris ZL. Aceruloplasminemia: an inherited neurodegenerative disease with impairment of iron homeostasis. Ann N Y Acad Sci 2004;1012:299–305.
15. Cherukuri S, Tripoulas NA, Nurko S, Fox PL. Anemia and impaired stress-induced erythropoiesis in aceruloplasminemic mice. Blood Cells Mol Dis 2004;33:346–355.
16. Raabe BM, Artwohl JE, Purcell JE, Lovaglio J, Fortman JD. Effects of weekly blood collection in C57BL/6 mice. J Am Assoc Lab Anim Sci 2011;50:680–685.
17. Harris ZL, Durley AP, Man TK, Gitlin JD. Targeted gene disruption reveals an essential role for ceruloplasmin in cellular iron efflux. Proc Natl Acad Sci U S A 1999;96:10812–10817.
18. Yamamoto K, Yoshida K, Miyagoe Y, Ishikawa A, Hanaoka K, Nomoto S, Kaneko K, Ikeda S, Takeda S. Quantitative evaluation of expression of iron-metabolism genes in ceruloplasmin-deficient mice. Biochim Biophys Acta 2002;1588:195–202.
19. Patel BN, Dunn RJ, Jeong SY, Zhu Q, Julien JP, David S. Ceruloplasmin regulates iron levels in the CNS and prevents free radical injury. J Neurosci 2002;22:6578–6586.
20. Schulz K, Vulpe CD, Harris LZ, David S. Iron efflux from oligodendrocytes is differentially regulated in gray and white matter. J Neurosci 2011;31:13301–13311.
21. Jiang R, Hua C, Wan Y, Jiang B, Hu H, Zheng J, Fuqua BK, Dunaief JL, Anderson GJ, David S, Vulpe CD, Chen H. Hephaestin and ceruloplasmin play distinct but interrelated roles in iron homeostasis in mouse brain. J Nutr 2015;145:1003–1009.
22. Wolkow N, Song D, Song Y, Chu ST, Hadziahmetovic M, Lee JC, Iacovelli J, Grieco S, Dunaief JL. Ferroxidase hephaestin's cell-autonomous role in the retinal pigment epithelium. Am J Pathol 2012;180:1614–1624.
23. Jiang B, Liu G, Zheng J, Chen M, Maimaitiming Z, Chen M, Liu S, Jiang R, Fuqua BK, Dunaief JL, Vulpe CD, Anderson GJ, Wang H, Chen H. Hephaestin and

ceruloplasmin facilitate iron metabolism in the mouse kidney. Sci Rep 2016;6:39470.
24. Yanagawa T, Itoh K, Uwayama J, Shibata Y, Yamaguchi A, Sano T, Ishii T, Yoshida H, Yamamoto M. Nrf2 deficiency causes tooth decolourization due to iron transport disorder in enamel organ. Genes Cells 2004; 9:641–651.
25. Zhao L, Hadziahmetovic M, Wang C, Xu X, Song Y, Jinnah HA, Wodzinska J, Iacovelli J, Wolkow N, Krajacic P, Weissberger AC, Connelly J, Spino M, Lee MK, Connor J, Giasson B, Harris ZL, Dunaief JL. Cp/Heph mutant mice have iron-induced neurodegeneration diminished by deferiprone. J Neurochem 2015;135:958–974.
26. Hahn P, Qian Y, Dentchev T, Chen L, Beard J, Harris ZL, Dunaief JL. Disruption of ceruloplasmin and hephaestin in mice causes retinal iron overload and retinal degeneration with features of age-related macular degeneration. Proc Natl Acad Sci U S A 2004;101:13850–13855.
27. Hadziahmetovic M, Dentchev T, Song Y, Haddad N, He X, Hahn P, Pratico D, Wen R, Harris ZL, Lambris JD, Beard J, Dunaief JL. Ceruloplasmin/hephaestin knockout mice model morphologic and molecular features of AMD. Invest Ophthalmol Vis Sci 2008;49:2728–2736.
28. Johnson LR, Ghishan FK, Kaunitz JD, Merchant JL, Said HM, Wood JD. Physiology of the gastrointestinal tract. Set. 5th ed. San Diego: Academic Press Imprint, Elsevier Science & Technology Books, 2012.
29. Takeuchi K, Bjarnason I, Laftah AH, Latunde-Dada GO, Simpson RJ, McKie AT. Expression of iron absorption genes in mouse large intestine. Scand J Gastroenterol 2005;40:169–177.
30. Frazer DM, Wilkins SJ, Darshan D, Mirciov CSG, Dunn LA, Anderson GJ. Ferroportin is essential for iron absorption during suckling, but is hyporesponsive to the regulatory hormone hepcidin. Cell Mol Gastroenterol Hepatol 2017;3:410–421.
31. Lee GR, Nacht S, Lukens JN, Cartwright GE. Iron metabolism in copper-deficient swine. J Clin Invest 1968; 47:2058–2069.
32. Craven CM, Alexander J, Eldridge M, Kushner JP, Bernstein S, Kaplan J. Tissue distribution and clearance kinetics of non-transferrin-bound iron in the hypotransferrinemic mouse: a rodent model for hemochromatosis. Proc Natl Acad Sci U S A 1987;84:3457–3461.
33. Osaki S, Johnson DA, Frieden E. The possible significance of the ferrous oxidase activity of ceruloplasmin in normal human serum. J Biol Chem 1966;241:2746–2751.
34. Osaki S, Johnson DA. Mobilization of liver iron by ferroxidase (ceruloplasmin). J Biol Chem 1969; 244:5757–5758.
35. Trenor CC 3rd, Campagna DR, Sellers VM, Andrews NC, Fleming MD. The molecular defect in hypotransferrinemic mice. Blood 2000;96:1113–1118.
36. Bartnikas TB, Andrews NC, Fleming MD. Transferrin is a major determinant of hepcidin expression in hypotransferrinemic mice. Blood 2011;117:630–637.
37. Kilkenny C, Browne WJ, Cuthill IC, Emerson M, Altman DG. Improving bioscience research reporting: the ARRIVE guidelines for reporting animal research. PLoS Biol 2010;8:e1000412.
38. el Marjou F, Janssen KP, Chang BH, Li M, Hindie V, Chan L, Louvard D, Chambon P, Metzger D, Robine S. Tissue-specific and inducible Cre-mediated recombination in the gut epithelium. Genesis 2004;39:186–193.
39. Frazer DM, Vulpe CD, McKie AT, Wilkins SJ, Trinder D, Cleghorn GJ, Anderson GJ. Cloning and gastrointestinal expression of rat hephaestin: relationship to other iron transport proteins. Am J Physiol Gastrointest Liver Physiol 2001;281:G931–G939.
40. Darshan D, Frazer DM, Wilkins SJ, Anderson GJ. Severe iron deficiency blunts the response of the iron regulatory gene Hamp and pro-inflammatory cytokines to lipopolysaccharide. Haematologica 2010;95: 1660–1667.
41. Frazer DM, Wilkins SJ, Mirciov CS, Dunn LA, Anderson GJ. Hepcidin independent iron recycling in a mouse model of beta-thalassaemia intermedia. Br J Haematol 2016;175:308–317.
42. Frazer DM, Wilkins SJ, Becker EM, Vulpe CD, McKie AT, Trinder D, Anderson GJ. Hepcidin expression inversely correlates with the expression of duodenal iron transporters and iron absorption in rats. Gastroenterology 2002;123:835–844.
43. Perls M. Nachweis von Eisenoxyd in gewissen Pigmenten. Virchow Arch Pathol Anat 1867;39:42–48.
44. Stevens AR Jr, White PL, Hegsted DM, Finch CA. Iron excretion in the mouse. J Biol Chem 1953;203: 161–165.
45. Frazer DM, Wilkins SJ, Becker EM, Murphy TL, Vulpe CD, McKie AT, Anderson GJ. A rapid decrease in the expression of DMT1 and Dcytb but not Ireg1 or hephaestin explains the mucosal block phenomenon of iron absorption. Gut 2003;52:340–346.

Received February 14, 2018. Accepted June 19, 2018.

Correspondence
Address correspondence to: Chris D. Vulpe, MD, PhD, Center for Environmental and Human Toxicology, 2187 Mowry Drive, Building 470 Room 113, University of Florida, Gainesville, Florida 32611. e-mail: cvulpe@ufl.edu; fax: (352) 392-2938.

Author contributions
BKF, YL, DD, DMF, SJW, and LD performed experiments; BKF, YL, and DMF analyzed data; BKF and AVL performed statistical analyses; SCK, JLD, PM, and HC provided consultation; BKF wrote the manuscript; BKF, GJA, and CDV conceived the work and designed experiments; and BKF, GJA, DMF, and CDV edited the manuscript.

Conflicts of interest
The authors disclose no conflicts.

Funding
Supported by research funding from the National Institutes of Health (NIH)/NIGMS, http://www.nih.gov, grant number 1R01GM083198-01A1 to CDV; the California Agricultural Experiment Station, University of California, Berkeley through NIFA Hatch Project CA-B-NTS-0020H to CDV; the Australian Research Council, www.arc.gov.au, grant number DP120103746 to GJA and CDV; the NIH (NEI), grant number EY015240, to JLD; and the National Science Foundation graduate research fellowship to BKF. GJA was the recipient of a Senior Research Fellowship from the National Health and Medical Research Council of Australia. The funders had no role in study design, data collection and analysis, decision to publish, or preparation of the manuscript.